HAL

archives-ouvertes.fr

New Statistical Methods for Precipitation Bias Correction Applied to WRF Model Simulations in the Antisana Region (Ecuador)

María Belén Heredia, Clémentine Junquas, Clémentine Prieur, Thomas Condom

▶ To cite this version:

HAL Id: hal-01971425
https://hal.archives-ouvertes.fr/hal-01971425

Submitted on 28 Jan 2019

New statistical methods for precipitation bias correction applied to WRF model simulations in the Antisana Region (Ecuador)

María Belén Heredia*, Clémentine Junquas [†], Clémentine Prieur [‡], Thomas Condom [§]

[*]*Corresponding author address:* ETNA, Irstea Grenoble, Saint-Martin-d'Hères, France

E-mail: maria-belen.heredia@irstea.fr

[†]Université de Grenoble Alpes, IRD, CNRS, IGE, F-38000 Grenoble, France

[‡]Université de Grenoble Alpes, CNRS, Inria Project/Team AIRSEA, Grenoble, France

[§]Université de Grenoble Alpes, IRD, CNRS, IGE (UMR 5001), F-38000 Grenoble, France

ABSTRACT

The Ecuadorian Andes are characterized by a complex spatiotemporal variability of precipitation. Global circulation models do not have sufficient horizontal resolution to realistically simulate the complex Andean climate and in situ meteorological data are sparse; thus, a high-resolution gridded precipitation product is needed for hydrological purposes. The region of interest is situated in the center of Ecuador and covers three climatic influences: the Amazon basin, the Andes and the Pacific coast. Therefore, regional climate models are essential tools to simulate the local climate with high spatiotemporal resolution; this study is based on simulations from the Weather Research Forecasting (WRF) model. The WRF model is able to reproduce a realistic precipitation variability in terms of the diurnal cycle and seasonal cycle compared to observations and satellite products; however, it generated some nonnegligible bias in the region of interest. We propose two new methods for precipitation bias correction of the WRF precipitation simulations based on in situ observations. One method consists of modeling the precipitation bias with a Gaussian process metamodel. The other method is a spatial adaptation of the cumulative distribution function transform approach, called CDF-t, based on Voronoï diagrams. The methods are compared in terms of precipitation occurrence and intensity criteria using a cross-validation leave-one-out framework. In terms of both criteria the Gaussian process metamodel approach yields better results. However, in the upper parts of the Andes (>2000 m), the spatial CDF-t method seems to better preserve the spatial WRF physical patterns.

2

1. Introduction

The Andes Cordillera forms a natural orographic barrier along the western coast of the South American continent, causing a complex spatiotemporal distribution of precipitation (e.g., Garreaud 1999; Espinoza et al. 2009). The spatial precipitation distribution is characterized by strong elevational gradients, with the eastern and western sides of the Andes exhibiting higher precipitation values than the high-elevation mountain peaks where the climate is relatively dry (see Fig. 1; e.g., Bendix and Lauer 1992). We distinguish three different climate regions in Ecuador: the Pacific coast, the Andes and the Amazon. Each side of the Andes is influenced by different atmospheric processes. The western plains of Ecuador are strongly influenced by the sea surface temperature variability of the Pacific Ocean. For instance the occurrence of ENSO (El Niño Southern Oscillation) events on an interanual timescale produces strong temperature and precipitation anomalies and significant socioeconomic issues (e.g., Rossel et al. 1999; Vuille et al. 2000; Rabatel et al. 2013; Vicente-Serrano et al. 2017). In the eastern part of the Andes, the moisture mainly comes from the Atlantic Ocean and water recycling through evapotranspiration over the humid Amazonian rainforest plains. In the Andes the interanual precipitation variability is influenced by both tropical Pacific and Atlantic sea surface temperature anomalies (e.g. Vuille et al. 2000; Espinoza et al. 2011). On the seasonal timescale, the precipitation variability is very complex and can be characterized by one or two rainfall seasons. On the Pacific coast, one rainfall season is generally described (e.g., Bendix and Lauer 1992; Vicente-Serrano et al. 2017) whereas two rainfall seasons are observed in most parts of the Andes (e.g., Bendix and Lauer 1992; Vicente-Serrano et al. 2017) and in the Amazon plains of Ecuador (e.g., Laraque et al. 2007; Espinoza et al. 2009) and these rainfall seasons occur from March to May, and from October to December. At the regional scale, these two periods correspond to the two annual transition phases of the American monsoon cy-

3

cle, between the mature phases of the North American monsoon system (June to August) and the South American moonson System (December to February; e.g., Vera et al. 2006). However, there are large disparities at the local scale (e.g., Laraque et al. 2007), due to local atmospheric processes associated with the complex orography of the Andes. The slope of the eastern part of the Andes is also characterized by the presence of local maximum precipitation values called "hotspots" (Espinoza et al. 2015), and in these regions the elevational gradients are nonlinear, with the maximum values situated between 500 and 2000 m. Thus, the spatiotemporal variability of precipitation is quite complex in this area, making it challenging to characterize with statistical models.

The Antisana glacier culminates at approximately 5760 m, and is located close to the Amazon slope on the eastern side of the Ecuadorian Andes. Quito, the capital of Ecuador, is situated approximately 50 km further west closest to the Pacific side of the Andes. The Antisana region is an important water reserve for the population (Chevallier et al. 2011; Hall et al. 2012; Basantes-Serrano 2015; Buytaert et al. 2017; Pouget et al. 2017). The water resources in this region depend in part on the Antisana glacier, whose mass balance is influenced by several factors, including precipitation variability, (e.g., Favier et al. 2004; Sicart et al. 2011). Recently, a dry trend has been identified in the western Amazon during the last decades, including in the Ecuadorian Amazon, and is particularly strong during austral winter (Espinoza et al. 2009). However, the station density in the Andes is low relative to the complexity of the topography, so the spatial distribution of precipitation is poorly understood (Buytaert et al. 2006; Rollenbeck and Bendix 2011; Manz et al. 2017). Precipitation in the highest elevation zones is particularly uncertain, as there are few stations located above 3500 m (see Fig. 1 and Table 1). Thus, to understand how the water resources of this region might change in the future, an essential first step is to establish a spatially complete picture of current-day precipitation.

4

In the Andes, global circulation models (GCMs) do not have sufficient horizontal resolution to realistically simulate the complex Andean climate (IPCC 2013). For this reason, regional climate models (RCMs) are essential for simulating the local climate with high spatiotemporal resolution. In this study the Weather Research Forecasting (WRF) model is used. Several previous studies have used the WRF model in the Andes, including, the works developed by Ochoa et al. (2014), Ochoa et al. (2016), Mourre et al. (2016), Junquas et al. (2017). Mourre et al. (2016) and Ochoa et al. (2016), compared WRF simulations to rainfall products derived from satellite products and in situ stations in the Peruvian Andes and in the Ecuadorian Andes, respectively. Whereas the WRF model is able to reproduce a realistic precipitation variability in terms of the diurnal cycle and seasonal cycle compared to observations and satellite products, these studies have also identified quantitative precipitation biases in the Andes, in terms of intensity (precipitation amounts) and occurrence (rainy/non-rainy days). Thus, before using WRF outputs in climate impact studies, the application of bias correction methods of the simulated precipitation is crucial (Vrac and Friederichs 2015).

In the Andes the orographic gradients play an important role on the atmospheric processes. The WRF model is able to reproduce two different spatial-scale mechanisms associated with the precipitation distribution (e.g., Ochoa et al. 2014; Mourre et al. 2016; Junquas et al. 2017): local-scale (e.g., valley and mountain winds) and synoptic-scale (e.g. low-level jet east of the Andes) circulation. The three previously defined climate regions in Ecuador (Pacific coast, Andes, and Amazon) are differently affected by these processes. Therefore, it is reasonable to think that the precipitation biases simulated by the WRF model could also be affected differently by these different atmospheric processes in each climate region. Thus, it is crucial to develop different statistical methods taking into account this particular climate distribution, by focusing on the spatial precipitation bias distribution.

Our main objective in this study is to statistically correct the WRF outputs of precipitation at the daily timescale, during the two-year period in the Antisana region (2014-2015). Considering the unique climate characteristics of the region and the few observations, we decided to develop new methods by adapting statistical tools from the literature. The first method consists of modeling the precipitation bias with a Gaussian process. This approach is also known as kriging in geostatistics and takes into account the spatial statistical structure of a variable of interest. Several studies have been developed to correct the precipitation bias based on Gaussian process models. For example, Hanchoowong et al. (2012) developed a bias correction of radar rainfall based on the kriging approach in Thailand, Müller and Thompson (2013) performed a bias adjustment of satellite rainfall in Nepal, they used kriging to interpolate precipitation from in situ measures, and Mourre et al. (2016) performed a precipitation interpolation based on kriging using as external drift the WRF simulation in the Cordillera Blanca (Peru). In Ecuador, the kriging method was already tested as a spatial interpolation method on the Pacific coast (Ochoa et al. 2014) and in the highlands (Buytaert et al. 2006) with in situ stations. They showed that using kriging interpolation with elevation as the external drift significantly improved the performance of the method in these regions. In our study, the novelty of our approach is to apply tkriging to the daily precipitation bias instead of the precipitation amount, as is classically done. We will show that this adaptation is particularly useful in regions where different precipitation regimes coexist, as is the case in our region with the Amazon and Andean climates.

The second approach generalizes the quantile-quantile method (e.g., Déqué 2007) and is based on the cumulative distribution function transform (hereafter CDF-t) with Singularity Stochastic Removal approach developed by Vrac et al. (2016). The probabilistic approach "cumulative distribution function-transform" (hereafter CDF-t) has been used in many applications, including correction of the punctual daily wind speed and regional downscaling (e.g., Michelangeli et al.

2009; Vrac and Vaittinada 2017). This approach has also been applied to correct the biases of different atmospheric variables; such as temperature, precipitation and relative humidity (e.g., Colette et al. 2012; Vrac et al. 2012). Vrac et al. (2016) proposed a modification of the CDF-t method for bias correction, specifically designed for precipitation, called "Singularity Stochastic Removal" (hereafter SSR). The motivation for developing an approach specialized for precipitation is because of its particular property in terms of a large number of zeros (non-precipitation events) in a daily time step. The principal advantage of this approach is that it allows us to correct biases while avoiding separating the correction in terms of occurrence (number of rainy days) and intensity of precipitation (quantity of precipitation). Previously, the SSR approach has been used to correct heat waves over France, as implemented by Ouzeau et al. (2016), and in a multivariate quantile mapping bias correction context to correct surface meteorological variables from regional climate model outputs across a North American domain (Cannon 2017).

The CDF-t is a variant of the quantile-mapping technique, which consists of mapping a model output x with cumulative distribution function (CDF) F_X, to its corresponding observation y with CDF F_Y, through a function T (Piani et al. 2010; Vrac et al. 2016). More precisely, considering $T = F_{Y^{-1}} \circ F_X$, where F_Y^{-1} is the generalized inverse of F_Y, thus we obtain $y = T(x)$ in the sense that $F_Y = F_{T(X)}$ (y is distributed as $T(x)$).

Then, T can be modeled either parametrically or nonparametrically, and estimated from the data. If the data are stationary and consist of n independent realizations of x (*resp.* y), then T can be estimated by $F_{Y,n}^{-1} \circ F_{X,n}$ with $F_{X,n}$ (*resp.* $F_{Y,n}$) representing the empirical CDF of x (*resp. y*). In that case, the procedure is known as the empirical mapping procedure.

Usually, the CDF-t approach is used to correct model predictions for future periods. We propose in this paper a spatial adaptation of the CDF-t approach from a point scale correction to a correction on any grid point, partitioning the region of interest using a Voronoi diagram of the stations (see

7

Section 3 for more details). Voronoï diagrams, also known as Thiessen polygons, have been widely used in meteorological applications. As for example in (Buytaert et al. 2006), spatial interpolation of precipitation with Thiessen polygons in the south Ecuadorian Andes is performed. In (Ly et al. 2011), spatial interpolation is performed in the Ourthe and Ambleve catchments in Belgium.

This paper is organized as follows. In Section 2 we present the data used in the study and the WRF simulation characteristics. In Section 3 we describe the new methods of precipitation bias corrections. We analyze the results and the intercomparison between them in Section 4. Finally, we summarize the main results and conclude in Section 5.

2. Data

a. In situ data

We use daily data from 26 in situ meteorological stations with elevations that range from 1110 to 4812 m, during the 2014-2015 period. All of the stations with the exception of station 26 were installed and are managed by the National Service of Meteorology and Hydrology of Ecuador (INAMHI). The stations from the INAMHI are of a tipping bucket type, and the highest is station 17 at 4009 m. The INAMHI data quality is routinely controlled, using the standard procedures in use by Met services worldwide. Based on in situ observations, Francou et al. (2004) determined the snowfall/rainfall limit at 4900 m close to the snout of the Ecuadorian glaciers. This elevation corresponds to a temperature threshold equal to 0.5 °. All the stations from the INAMHI network are situated below 4009 m, so we do not observe snowfall at the INAMHI' stations (see Table 1). Station number 26, belonging to the SNO GLACIOCLIM, is situated at 4812 m. Snowfall is frequent at this altitude, and some care must be taken to reduce the uncertainty of the measurement. First, the gauge should be adapted to measure any type of hydrometeor (solid or liquid). Second

8

the problem of undercatch, principally caused by wind must be addressed. In the present study, we used data issued from Geonor gauge; this type the gauge is a weighting device specifically designed to measure all the hydrometeor types and is suitable for both solid and liquid precipitation. To reduce the problem of under catch principally caused by wind effects, we use the correction proposed by Forland et al. (1996), depending on the air temperature and wind velocity. The detailed procedure for the data treatment is provided in Wagnon et al. (2009). At the regional scale for the whole Andean zone defined in the study, the snowfalls are not very important if one considers the surface of the ground located higher than 4900 m (less than 1% of the total area).

Figure 1 shows a map with the locations of the stations. The study area is divided into three regions corresponding to three regions of Ecuador (see Section 1): the region located on the Pacific coast side (hereafter Pacific coast) formed by stations 2, 22 and 23; the Amazon formed by stations 19 and 25; and the Andes, formed by the remaining ones (21 stations). Most stations are located in the Andes (81%), with 11% on the Pacific coast and 8% in the Amazon. Table 1 presents a description of the location and accumulated precipitation for the period 2014-2015 for each meteorological station. The meteorological stations located in the Amazon registered the highest total precipitation values (with total precipitation greater than 6000 mm in the two years).

Because very few in situ stations were available in this region, we included two stations (numbers 12 and 18) situated very close to the limits of the domain (less than 4km in latitude) and at the same elevation. Because the main idea of this study is to test bias correction methodologies, we decided to include these two stations for these tests, by assigning their corresponding model grid latitudes as 0.01 to avoid the boundary zone of the model (see Section 2c). Originally, station number 12 was situated at the latitude 0.05 and station number 18 was situated at the latitude 0.03, corresponding to 4km and 2km from the model limit, respectively. We performed statistical analysis (not shown) that confirmed that these precipitation timeseries of the WRF-1km grid

9

points are significantly correlated to the corresponding in situ stations timeseries in terms of occurrence and intensity, even considering some km lags, highlighting that precipitation variability is homogeneous in this small region.

b. CHIRPS satellite product

Satellite-based rainfall estimates such as CHIRPS (Climate Hazard Group 1981; Funk et al. 2015) provide an opportunity for a wide range of hydrological applications, from water resource modeling to monitor of extreme events, such as droughts and floods. CHIRPS is a continental rain data set that combines satellite and rain gauges data with a spatial resolution of $0.05° \times 0.05°$. CHIRPS uses the global cold cloud duration (CCD) as a thermal infrared method to estimate the global precipitation. Then, the product TRMM-3B42 V7 is used to calibrate the precipitation estimated by the global CCD. Finally, gauge stations are used to calibrate the estimations of precipitation (Paccini et al. 2018). Recent studies note that, at daily time steps or for arid environments, important biases exist in these rainfall estimations (Herold et al. 2017; Paredes-Trejo et al. 2017). Furthermore, Bai et al. (2018) used the CHIRPS product in mountainous regions in China and concluded that the ability of CHIRPS to detect snowfall was limited. More generally, this product has known biases, including underestimation of extreme precipitation events (Funk et al. 2015). In our study, the use of the precipitation satellite product CHIRPS for the period of 2014-2015 allows for a graphical evaluation of the corrected gridded precipitation products. Indeed, this product provides good spatial patterns at seasonal or annual scales (Zambrano-Bigiarini et al. 2017). Thus, we use this dataset for a spatially complete qualitative comparison, but only in an approximate sense.

c. WRF simulation and its biases

₂₁₇ The WRF model version 3.7.1 (Skamarock et al. 2008) is used to simulate high-resolution pre-

₂₁₈ cipitation for the period 2014-2015 in the studied region. The model is nonhydrostatic and uses

₂₁₉ a terrain-following vertical coordinate (sigma). The WRF model is established with 4 one-way

₂₂₀ nested domains (27 km, 9 km, 3 km, and 1 km; see Fig. 2). The outer domain is forced by the

₂₂₁ NCEP-FNL reanalyses ($1° \times 1°$). The simulation outputs of the innermost domain (1km $\times$1km)

₂₂₂ are used for this study. The in situ data for each station are compared with the closest 1km grid

₂₂₃ point of the WRF simulation. As mentioned in Section 2a, for two stations (numbers 12 and 18),

₂₂₄ the closest inner-domain gridpoint was considered to avoid the northern lateral boundary zone of

₂₂₅ the model (5 gridpoints of specified and relaxation zone; see Fig. 2d). The four domains are con-

₂₂₆ figured with 30 sigma levels in the atmosphere, and the top model is configured at 50hPa, as it was

₂₂₇ already used in previous studies in the tropical Andes (Junquas et al. 2017; Moya-Álvarez et al.

₂₂₈ 2018). The output time resolutions are 6 h, 3 h, 3 h, and 1 h for the first, second, third and fourth

₂₂₉ domain, respectively.

₂₃₀ Some options for the dynamical and physical parameterizations were previously tested to pro-

₂₃₁ vide better precipitation results in the region of interest (not shown). The chosen parameterizations

₂₃₂ are described as follows. We use the Yonsei University scheme (Hong et al. 2006) as the plane-

₂₃₃ tary boundary layer option, with a wind topographic correction for the complex surface terrain

₂₃₄ (Jiménez and Dudhia 2012), that has already been used in previous studies using the WRF model

₂₃₅ in the Andes (Mourre et al. 2016; Junquas et al. 2017). The Microphysical parameterization is

₂₃₆ from Lin et al. (1983), and the cumulus scheme is from Grell and Dévényi (2002). Preliminary

₂₃₇ tests have been performed with other parameterizations, and this configuration was chosen be-

₂₃₈ cause the precipitation bias in the Andes was less pronounced (not shown). We decided to employ

the cumulus parameterization in the four domains because in our tests, the convection-permitting experiment (no cumulus scheme activated at 3 km and 1 km) exhibit the greatest bias with a precipitation overestimation of more than 300% in the Andes compared to station data (not shown). This result confirms the results of a recent paper that did not find precipitation improvements using convection permitting in WRF forecasting simulations in the Peruvian Andes region (Moya-Álvarez et al. 2018).

As the surface model, we use the Noah multi-physics model with a snow option (snf_opt=2; Niu et al. 2011; Yang et al. 2011) as previously tested in the Cordillera Blanca in Peru (Mourre et al. 2016). The longwave and shortwave radiation options are RRTM (Mlawer et al. 1997) and Dudhia scheme (Dudhia 1989), respectively. The surface layer parameterization is MM5 similarity (Paulson 1970). We used the SRTM (Shuttle Radar Topography Mission; Farr et al. 2007) digital elevation model instead of the USGS (United States Geological Survey) data as topographic forcing, as suggested by preliminary studies.

We compared the in situ observations and the WRF simulations and found that they are biased (see Figure 3). The mean bias per station is 1.89 mm day^{-1} during the two years with, a minimum of 0.04 mm day^{-1} (achieved at station 17) and a maximum of 9.72 mm day^{-1} (station 2). During 2014, the mean relative bias is an underestimation of 20%, its maximum underestimation is 80% (station 2) and the maximum overestimation is registered at station 6 (47%). During 2015, the mean relative bias is an underestimation of 42%, with a maximum underestimation of 85% (station 2), and the maximum overestimation is 23%, registered at station 13.

The biases are more evident in the Amazon, where underestimations of approximately 8.20 and 6.96 mm day^{-1} are obtained for stations 19 and 25. The biases of the 2014 and 2015 periods are slightly different because during 2014, there is strong overestimation of the simulated precipitation at some stations of the Andes (stations 3, 6 and 18), in contrast to 2015, when underestimation are

12

obtained for most of the stations (except for 13 and 17). It is clear from these figures that the spatial bias variability strongly depends on the period under consideration. The spatial distribution of the bias in 2015 (Fig. 3b) appears more homogeneous than the one in 2014 (Fig. 3a). This contrast is explained by different local influences of atmospheric processes on the interannual variability in the region of the Andes. The interannual variability is part of the complexity of the spatiotemporal precipitation distribution in the Ecuadorian Andes. Note that some biases identified in the WRF simulations could potentially be caused by errors in the in situ observations.

3. Bias correction methods

Two methods for bias correction are adapted and analyzed in this study. The first one is to model the WRF bias with a Gaussian process model, also known as kriging, and the second one is a time series preprocessing and spatial adaptation of the CDF-t method. The methods are described in this section (parts a and b), and we present the criteria used to evaluate the performance of the two approaches that are used (part c) in the results section (Section 4).

a. Gaussian process modeling

The first method implemented is to model the WRF biases using a Gaussian process model; Figure 4 presents the flowchart of our method. In the following, we define bias as follows:

$$\text{BIAS} = \text{WRF simulation} - \text{Observation}. \tag{1}$$

Then, at in each point where there is no observation, we obtain a prediction of the bias ($\widehat{\text{BIAS}}$) and we compute the predicted precipitation ($\widehat{\text{Precip.}}$) value as follows:

$$\widehat{\text{Precip.}} = \text{WRF simulation} - \widehat{\text{BIAS}}. \tag{2}$$

13

We refer to the work of Marrel et al. (2008) for a presentation of Gaussian process modeling (also see the work of Oakley and O'Hagan (2002)). Consider that n observations of a phenomenon are registered at n different locations (for example, the bias precipitation registered in n stations of the region under study). We consider in the following that each observation $y(x)$ is registered at point $x = (x_1, x_2) \in \mathbb{R}^2$ (the coordinates of x correspond to the longitude and latitude of the station), endowed with the usual Euclidean distance. The set of points where the observations are collected is denoted by $x_s = (x^{(1)}, ..., x^{(n)})$ with $x^{(1)}, ..., x^{(n)} \in \mathbb{R}^2$ (in our study, each x corresponds to a station). The set of observations of the phenomenon is denoted by $y_s = (y^{(1)}, ..., y^{(n)})$ with $y^{(i)} = y(x^{(i)})$. The Gaussian process modeling consists of representing $y(x)$ as a realization of a random function $Y(x)$ such that:

$$Y(x) = f(x) + Z(x) + U(x), \tag{3}$$

where $Z(x)$ is a centered stationary Gaussian process; $U(x)$ represents the noise in the observations and is a centered stationary Gaussian process with a diagonal covariance structure; and $f(x)$ is a deterministic function that represents the tendency, also known as the external drift, linear combinations of longitude, latitude and elevation are commonly used. More generally, it is constructed as a finite linear combination of k elementary functions:

$$f(x) = \sum_{j=0}^{k} \beta_j f_j(x) = F(x)\beta \tag{4}$$

where $\beta = (\beta_0, ..., \beta_k)^T$ is the regression parameter vector and $F(x) = (f_0(x), ..., f_k(x))$. The function $f(x)$ allows the addition of an external drift into the modeling, and this is advantageous because it allows a nonstationary global modeling framework; in other words the variable Y does not need to be stationary but the variable Z is assumed to be stationary.

The Gaussian centered process $Z(x)$ has the following a covariance function:

$$\text{Cov}(Z(x), Z(u)) = K(x - u) = \sigma^2 R(x - u), \tag{5}$$

where $x, u \in \mathbb{R}^2$ (in our application, u also corresponds to the coordinates longitude and latitude of a station), σ^2 is the variance of Z, and R is its correlation function. The process Z is stationary because it is considered that its correlation function depends only on the difference between x and u.

In this study, we used the Matérn covariance functions because they are stationary and commonly used in spatial statistics studies due to their flexibility (Paciorek and Schervish 2006); and they are defined follows:

$$K(x, u) = \frac{1}{\Gamma(\nu) 2^{\nu-1}} \left[\frac{\sqrt{2\nu}}{\kappa} |x - u| \right]^\nu K_\nu \left(\frac{\sqrt{2\nu}}{\kappa} |x - u| \right), \tag{6}$$

where K_ν is the modified Bessel function of second kind of order $\nu > 0$, κ is a positive parameter that represents the characteristic length scale and Γ is the Gamma function (Rasmussen and Williams 2005). The Euclidean distance, written as $|x - u|$, is used.

The aim of Gaussian process modeling is to estimate the prediction of Y for a new grid point x^*. In our study, Gaussian process modeling is applied to estimate the bias at grid points at which there is no station. In our application, first, the bias is computed for annual averages to assess the accuracy of four models constructed by the combination of three commonly used drifts (longitude; latitude and elevation) and to choose one of them. Here-after, they are referred to as the GP model with drift longitude, latitude and elevation (GP+longitude+latitude+elevation), the GP model with drift longitude and latitude (GP+longitude+latitude), the GP model with drift longi-

15

₃₁₈ tude (GP+longitude) and the GP model with drift elevation (GP+elevation). Then, we computed

₃₁₉ the daily bias using the GP with the selected drift to obtain a corrected daily precipitation product.

b. Spatial adaptation of the CDF-t method

₃₂₁ Historically, the CDF-t method has been applied as a statistical downscaling method and to

₃₂₂ correct future time series from GCMs outputs. In our study, the CDF-t method aims at relating

₃₂₃ CDFs of a climate variable (here the precipitation) from WRF simulation outputs to the CDF of

₃₂₄ this variable from the in situ observation. However, instead of applying the correction over future

₃₂₅ time series, we adapt the method to correct the gridpoints of the domain, even where there is no

₃₂₆ associated observation. We call this approach a spatial adaptation of the CDF-t method. The main

₃₂₇ idea is to partition the region under study (see Fig. 1) into neighboring sub-regions, in such a

₃₂₈ manner that every subregion contains a station. We are going to assume that the precipitation

₃₂₉ biases in these subregions behave similarly.

₃₃₀ To define the subregions, we divide the region using a partition based on Voronoï diagrams.

₃₃₁ This method is a simple way to define subregions, that is, applicable to any mountain region with

₃₃₂ few complete in situ precipitation time series, as in our case. In addition, as there is no spatial

₃₃₃ smoothing, it has the advantage of conserving the spatial coherence of the physical processes

₃₃₄ simulated by the WRF model inside each subregion. Another advantage of using Voronoï diagrams

₃₃₅ is their simplicity and low computational cost, which allow them to be used with large volumes of

₃₃₆ data.

₃₃₇ At a given station s, let us denote X_t^s the model simulation at time t and Y_t^s its corresponding

₃₃₈ observation. The time series under study are nonstationary and autocorrelated, hence the standard

₃₃₉ empirical mapping cannot be used directly (see Section 1). Indeed, we performed the usual statisti-

₃₄₀ cal hypothesis testing procedures to detect nonstationarity: the Kwiatkowski Phillips Schmidt Shin

16

test (Kwiatkowski et al. (1992); KPSS where H_0 : The time series is stationary), and the Mann-Kendall test (Mann (1945); Kendall (1948); H_0 : The time series do not have a monotonic trend). The p-value results of the KPSS and Mann-Kendall tests are less than 0.1 and 0.05, respectively, for all the observed and simulated time series, meaning that the time series are nonstationary due to a unit root (autocorrelation close to 1) and dependent. It is thus necessary to perform differentiation and subsampling. More precisely, we applied the following preprocessing: we calculated $\Delta X_t^s = X_t^s - X_{t-1}^s$ and $\Delta Y_t^s = Y_t^s - Y_{t-1}^s$ to stationarize the time series, and we used subsampling to eliminate the autocorrelation. The manner in which we performed subsampling is the following: as the autocorrelation length was estimated to $k = 2$, we skipped one observation out of two.

As already mentioned, the main issues of bias correction for precipitation data is the treatment of the rainfall occurrences. To solve this issue Vrac et al. (2016) proposed changing the null precipitation data for a uniform distribution. In our case, we corrected the differentiated time series of precipitation, thus we adapted the SSR to our framework. More precisely, we performed the following steps on our data:

Step 1.- Determinate a threshold θ such that:

$$\theta = \min \left(\inf_{t \geq 1, |\Delta X_t^s| \neq 0} \{|\Delta X_t^s|\}, \inf_{t \geq 1, |\Delta Y_t^s| \neq 0} \{|\Delta Y_t^s|\} \right) \tag{7}$$

Step 2.- Each time $\Delta X_t^s = 0$ (*resp.*, $\Delta Y_t^s = 0$), we simulate a value v from the uniform distribution $U[-\theta, \theta]$ and we replace ΔX_t^s (*resp.*, ΔY_t^s) with the sampled value.

Such a step avoids separating the correction of the occurrences from the one of the intensities. (Vrac et al. 2016).

17

Step 3.- Nonparametrically estimate the mapping $F_{\Delta Y^s}^{-1}(F_{\Delta X^s})$ using e.g., the R package developed by Vrac (2015) (see also Michelangeli et al. (2009)). The mapping will be denoted by $\widehat{T}^s$ in the following.

In this paper, we do not aim at correcting the bias for future predictions, but we want to correct the bias at any grid point where no observation is available.

Therefore, we construct a Voronoï diagram based on seeds composed with the stations. For each station (seed) there is a corresponding region consisting of all points closer to that seed than to any other. In this manner, we obtain as many regions as the initial number of stations, let us say $\mathscr{S}$. For $s = 1, \ldots, \mathscr{S}$, we construct following Step 3 a mapping $\hat{T}^s$ from time series X_t^s and Y_t^s. We then assume that the mapping is constant on each Voronoï cell. We then proceed with the following steps:

Step 4.- At any grid point, let us consider the closest station s. We consider the time series ΔZ_t, where Z_t denotes the WRF simulation at time t. If the grid point coincides with station s, then $Z_t = X_t^s$). We apply the following bias correction:

$$V_t = Z_{t-1} + \hat{T}^s(\Delta Z_t) \tag{8}$$

Step 5.- The bias corrected data V_t lower than θ are set to 0. This step allows us to recover the correct occurrence of 0 precipitation.

As an illustration of the procedure, Figure 5 shows for 3 stations (one for each region) the original time series (X_t and Y_t), the differentiated ones (ΔX_t and ΔY_t) and the CDFs of the observation, simulation and CDF-t correction (more details are presented in Section 4b).

18

c. Evaluation criteria to compare the two approaches

₃₈₀ To compare the accuracy of the rainfall products created by these two methods (Gaussian pro-

₃₈₁ cess modeling and spatial CDF-t approach), we have computed various criteria concerned with

₃₈₂ occurrences (number of rainy/non-rainy days) and intensity of precipitation (precipitation quan-

₃₈₃ tity). These criteria are commonly used in the literature; for example, they were used in the works

₃₈₄ of Maussion et al. (2011), Ochoa et al. (2014), Mourre et al. (2016) and, Vrac et al. (2016).

₃₈₅ CRITERIA RELATED TO THE OCCURRENCE

₃₈₆ A day is considered as a "rainy day" if its daily precipitation value is greater than 1 mm day^{-1}.

₃₈₇ Note that other threshold values were tested, but the best agreement between the WRF model

₃₈₈ and in situ observations was obtained with 1 mm day^{-1} (not shown). In the following, several

₃₈₉ measures that depend on the following four major parameters are used:

₃₉₀ **True Positive (TP)**: Rainy day identified by WRF as a rainy day.

₃₉₁ **True Negative (TN)**: Non-rainy day identified by WRF as a non-rainy day.

₃₉₂ **False Positive (FP)**: Non-rainy day identified by WRF as a rainy day.

₃₉₃ **False Negative (FN)**: Rainy day identified by WRF as non-a rainy day.

₃₉₄ The false alarm rate (FAR) is defined as the incorrect number of rainy days simulated divided

₃₉₅ by the total number of rainy days simulated:

$$FAR = \frac{\#FP}{\#FP + \#TP} \tag{9}$$

₃₉₆ The probability of detection (POD) is defined as the ratio between the number of rainy days

₃₉₇ simulated correctly and the total number of rainy days observed:

$$POD = \frac{\#TP}{\#TP + \#FN} \tag{10}$$

The probability of false detection (PODF) is the ratio between the number of rainy days incorrectly simulated to the number of non-rainy days of the observation:

$$PODF = \frac{\#FP}{\#FP + \#TN} \tag{11}$$

And finally, the Heidke skill score (HSS) is calculated as:

$$HSS = \frac{S - S_{ref}}{1 - S_{ref}}, \tag{12}$$

where $S = \frac{\#TP + \#TN}{n}$ and $S_{ref} = \frac{(\#TP + \#FP)(\#TP + \#FN) + (\#FP + \#TN)(\#FN + \#TN)}{n^2}$. It could be interpreted as the ability of the simulation to be better or worst than a random simulation. A perfect product should have a FAR value of 0, a POD value of 1, a 0 PODF value and an HSS value of 1.

CRITERIA RELATED TO THE INTENSITY

The following criteria are used to evaluate gridded products accuracy in terms of intensity: the Kolmogorov-Smirnov test (KS) is a nonparametric test to compare two distributions; the maximal difference between them is calculated. The Spearman correlation coefficient, the root mean square error (RMSE) and the mean bias are computed. It is important for the precipitation also to know the percentage of data that is greater than the 0.95 percentile of the observation and in the case of a good precipitation product, it should be close to 5% (here-after referred as Q_{95}). Finally, the predictivity squared correlation coefficient Q_2 is computed. It measures the predictive ability of

20

the statistical model.

$$\text{mean bias} = \frac{1}{n} \sum_{i=1}^{n} (\widehat{x}_i - x_i), \tag{13}$$

$$\text{RMSE} = \sqrt{\frac{1}{n} \sum_{i=1}^{n} (\widehat{x}_i - x_i)^2}, \tag{14}$$

$$Q_2 = 1 - \frac{\sum_{i=1}^{n} (x_i - \widehat{x}_i)^2}{\sum_{i=1}^{n} (\overline{x} - x_i)^2}, \tag{15}$$

where $\widehat{x}_i$ is the prediction of the precipitation (using one of the approaches described before) at station i, x_i is the observed precipitation at the same station i and $\overline{x}$ is the observed mean. These criteria should be computed on a set of stations independent from the ones used to learn the statistical model. However, we used all the stations to train the model (Gaussian Process or CDF-t); thus (13), (14) and (15) will be computed by cross-validation in the following. The leave-one-out cross-validation consists of splitting the data into two groups: a group composed with all the stations except one, which is used as learning sample, and another group whose sole element is the remaining station, on which the model is validated. Then, the procedure is averaged on all such leave-one-out splits. For example, for Q_2:

$$1 - \frac{\sum_{k=1}^{n} (x_k - \widehat{x}_k^{-(k)})^2}{\sum_{k=1}^{n} (\overline{x} - x_k)^2} \tag{16}$$

where $\widehat{x}_k^{-(k)}$ is the prediction at station number k, when the model is trained by the $n-1$ remaining stations.

4. Results

The principal results that we obtained are presented in this section. Subsections a and b are devoted to the results for the GP modeling and spatial CDF-t. In subsection c we present the

21

intercomparison between both approaches. All the analysis and methods implementation were performed in R (R Core Team 2015).

a. Gaussian process modeling

We implemented the GP models using the R package gstat developed in (Pebesma 2004; Gräler et al. 2016). We evaluated the four GP models to select an external drift using a cross-validation leave-one-out framework. Table 2 presents the cross-validation results for the four corrected precipitation gridded products. All of the four proposed GP models exhibit better results than the uncorrected WRF outputs in terms of the criteria of Section 3c (mean, bias, RMS and correlation; see Table 2). However, in general, the GP+longitude+latitude model obtains the best results in terms of all of the criteria (bias, RMSE, correlation and Q_2). In terms of predictability (Q_2), the GP+longitude+latitude model exhibits the highest values, but the GP+elevation model values are not significantly different. The GP+longitude+latitude+elevation model yields the lowest predictability values. Thus, this last model most likely overfits the data, whereas more parsimonious models have better predictive ability.

Analyzing the two years separately, it is found that the predictive ability is better in 2015 for the four models. However, for some criteria the values are not significantly different for each year, such as for RMSE values for GP+longitude and for GP+elevation. In addition, for the GP+elevation model the mean bias is higher for 2015 than for 2014. Longer periods are necessary to adequately analyze the choice of the external drift parameters on the results, which is beyond of the scope of this study considering that we only have available data spanning a two-year period. Therefore, we chose the GP+longitude+latitude model and used a Matérn covariance function to correct the daily precipitation by using separate daily variograms described in (Gräler et al. 2012) because this model yields the best results for both years of analysis. Figure 6a shows

22

the mean daily precipitation of the gridded products WRF and CHIRPS, and the cross-validation results of the GP compared to the mean daily precipitation of the station. Their respective linear regression lines are drawn. The R^2 value of the linear regression of WRF is 0.38, that of GP is 0.62 and that of CHIRPS is 0.70, which means that the results of the cross-validation of GP are better than WRF. Figures 7a,b,c show the accumulated precipitation of WRF, the GP correction in cross-validation and the precipitation registered at the three stations (Fig. 7a shows Pacific coast station 22; Fig. 7b shows Andes station 26, and Fig. 7c shows Amazon station 25). At the Pacific coast and the Andes stations, the corrections yield an overestimation of the precipitation (see Fig. 7a and Fig. 7b), and at the Amazon station, the correction increases the precipitation to correct the underestimation simulated by WRF (see Fig. 7c).

b. Spatial CDF-t

The procedure described in Subsection 3b is applied. The Voronoï diagram is calculated (see Fig.10f) and maps of mean of daily precipitation are presented in Fig. 10 (the stations), 10b (CHIRPS), 10c (WRF), 10d (GP) and 10e (CDF-t). The Voronoï diagram borders are marked in the Amazon due to the inhomogeneous distribution of the stations and also high underestimated precipitation in this region (for example, approximately 3000 mm year^{-1} at station 25). On the Pacific coast, the border of the polygon associated with station 22 is marked because it has recorded higher precipitation values. On the contrary, the polygon borders around the Andes are not visible in most of the cases because the biases in the Andes were quite homogeneous (see Figures 3a and 3b). Therefore, in the Andes, the spatial CDF-t approach yields realistic results, by conserving the precipitation physical gradients simulated by WRF. A homogeneous station distribution could increase the accuracy of the method by taking into account more physical variables in addition to geometrical properties. Figure 6b shows the mean daily precipitation of the gridded products

23

WRF, CHIRPS, and CDFt and their linear regression lines. The R^2 coefficient of CDFt (0.89) is better than that of WRF (0.38). Figures 7d,e,f shows the accumulated precipitation of WRF, the spatial CDF-t correction and the precipitation registered in the observation of three regions stations (Fig. 7d shows Pacific coast station 22; Fig. 7e, shows Andes station 26; and Fig. 7f Amazon station 25). At the Pacific coast station, the WRF simulation and its correction are similar; there is a slight increase in the precipitation in the correction to obtain a value closer to the observation (see Fig. 7d). The correction applied to the Andes station is also slight because the biases registered at these stations are low (see Fig. 7e). The correction for the Amazon station is more evident due to the high underestimation obtained by WRF (see Fig. 7f).

c. Intercomparison between the two methods

After analyzing separately the implementation of the spatial CDF-t approach and the GP correction methods, we now present the an intercomparison between these different bias corrections using cross-validation leave-one-out. We use the criteria from the Subsection 3c to compare the two correction approaches (GP and spatial CDF-t) and WRF. The GP model used for these results is GP+latitude+longitude, as it was shown to outperform the other GP models tested in Table 2.

The criteria related to the occurrence are shown in Figure 8. The spatial CDF-t method yields results similar to WRF in terms of the FAR (mean of 0.47 and 0.45, respectively) and PODF criteria (spatial CDF-t has a mean of 0.21 and WRF 0.23); meanwhile the GP result is worst (mean of 0.53 in FAR and 0.51 in PODF). The HSS results are similar for the three spatial products (WRF has a mean of 0.23, spatial CDF-t has 0.21 and GP has 0.22), and the HSS criterion is more stable for GP since its variance is less than those of the other products (GP has a standard deviation of 0.09, spatial CDF-t has 0.12, and WRF has 0.11, see Fig. 8d). The POD criterion is highly improved by GP (0.79 versus 0.49 for the Spatial CDF-t).

24

The results related to the precipitation intensity are shown in Figure 9. The KS criterion is improved with the spatial CDF-t (a mean of 0.21 versus 0.38 for GP) but the results exhibit a high variability (a standard deviation of 0.2, and GP has a standard deviation of 0.15). The RMSE criterion is similar for the two products (spatial CDF-t has a mean of 7.78, GP has 7.16, and WRF has 7.78). However, on the contrary, the Spearman correlation (GP has a mean of 0.38, versus 0.24 for spatial CDF-t) and Q_{95} (GP has a mean value of 0.05, versus 0.04 for spatial CDF-t) values are slightly improved in GP.

The CHIRPS daily mean map is displayed in Figure 10b. Because of well-known quantitative biases in the tropical Andes (up to 80%; e.g., Espinoza et al. (2015)), we use only this data to visually compare the spatial precipitation patterns. When visually comparing both corrected products, it seems that the GP model (Fig. 10d) is more similar to the satellite than the spatial CDF-t (Fig. 10e) in the Andes, mainly due to the sharp discontinuities at the polygon borders on the eastern slope. However, in the Amazon the GP model shows a zone of maximum precipitation in the south-east of the domain that is not observed in the satellite data. However, given that, the satellite data are biased and there are no data in this part of the region, this result could be uncertain. A strong gradient of precipitation is evident in the eastern slope of the Andes in both the GP model and the satellite data. This gradient depends on the elevation and the presence of local atmospheric valleys processes (e.g., Egger et al. (2005); Junquas et al. (2017)). Previous studies have found that the WRF model is able to reproduce some local valley processes in the tropical Andes (e.g., Mourre et al. (2016); Junquas et al. (2017)). Therefore, it is important to take into account that such WRF spatial patterns should be preserved in a bias correction method. This orographic limit is visually well represented with the GP method, compared with the satellite. Whereas the spatial CDF-t is visually unrealistic on the eastern slope of the Andes due to the polygon limits, in the Andes above 2000 m it seems to be able to conserve the spatial patterns of WRF. In addition, the CDF

25

of the WRF Antisana gridpoint is very similar to the Antisana station CDF (Fig. 5h), and the relative bias is very weak (Fig. 3). We then expect, that in this particular region, no large quantitative bias correction should be applied. However, whereas the spatial CDF-t clearly exhibits very little quantitative correction in this region, the GP model exhibits increased precipitation, generating an overestimation compared to the observations (see Fig. 7a and Fig. 7b). The spatial CDF-t method seems then to be adapted to the upper parts of the Andes (above about 2000 m), where relatively low precipitation values dominate compared to the Amazon precipitation. In the contrast, it is not recommended to use the spatial CDF-t in regions where strong precipitation gradient exists.

5. Conclusions and future work

The aim of this study was to correct the WRF simulation precipitation biases in the studied region. Then, the final gridded products of precipitation will be used as external forcing data for hydrological and glaciological models to understand water resources and glaciers evolution in the Andes. Therefore, two methods of precipitation bias correction were explored and adapted: the first one consisted of modeling the daily WRF biases through Gaussian process (GP) models, and the second one was based on a spatial and time series adaptation of the CDF-t method developed by Michelangeli et al. (2009) and Vrac et al. (2016).

First, four GP models were proposed by using four combinations of external drifts (generally used in studies of this type, including latitude, longitude and elevation variables) to model the annual accumulated bias during the years 2014 and 2015. The accuracy of the GP models was tested in a cross-validation leave-one-out framework. Based on four criteria (Bias, RMSE, Correlation and Q_2), the best model was GP with drift longitude and latitude. Thus, we chose this model to correct the daily precipitation by using separate daily variograms as it is described in (Gräler et al. 2012).

26

We employed the SSR method with a time series adaptation to obtain the CDF estimations and a spatial adaptation to obtain the correction in the region. The methods were compared in terms of criteria related to the occurrence (FAR, POD, PODF, and HSS) and criteria related to the intensity (mean bias, Spearman correlation, KS, RMSE, Q2, and Q_{95}). Compared with the WRF product, the spatial CDF-t approach did not exhibit significant changes, whereas the GP model correction increased the daily rain number and the total accumulated mean, improving (or worsening) significantly some intensity (occurrence) statistical scores. In terms of spatial distribution, when considering the entire WRF domain, including the three climate regions (Pacific coast, Andes, and Amazon), the GP correction yields a more realistic distribution than the spatial CDF-t, because of the marked polygon borders induced by this second method. However, at local scale in the Andes, the spatial CDF-t method seems to be more similar to the original WRF patterns.

In the Andes, the orography is an important factor that influences precipitation. Whereas, the GP model with elevation drift seems to be a good choice for mountainous regions, it was not found to be the best GP model considering our statistical scores. This could be because the majority of our observational data are from the high elevations of the Andes, above 2000 m. This result shows that above this limit, the spatial precipitation pattern is more complex than a simple orographic gradient. Previous studies working with the WRF model in tropical Andes regions have demonstrated the importance of both local mountain winds and synoptic conditions (e.g., Mourre et al. 2016; Junquas et al. 2017). In our study, the spatial CDF-t appears to be a bias correction method with a strong capacity for conserving the original spatial precipitation pattern (only considering the Andes above 2000 m). Therefore, depending on the bias characteristics of the WRF simulation, the region of study, and the intended application for the final product, one method or the other should be used for bias correction. If the bias correction is to be applied in a large region including various

27

climate characteristics with strong biases, the GP method would be recommended. Otherwise, if the region is a reduced domain with a relative uniform synoptic climate characteristics but strong influences of local atmospheric processes well represented by the model, the spatial CDF-t method would be preferred.

There is still work to be performed on the methods here presented to increase their accuracy. Thus, the perspectives of this study are the following: (i) to deeply analyze the implementation of stationary tests for a GP model, (ii) to develop the spatial CDF-t approach for a more complex spatialization strategy, including more than geometrical properties, as is the case for the Voronoï diagram. One alternative to the Voronoï diagram could be the use of a functional clustering meethod as in (Antoniadis et al. 2012) where a curve-based clustering is used to reduce the data dimension for constructing a metamodel for West African monsoon. The functional clustering method has the advantage of taking into account time-point correlations of time series spatial data (Antoniadis et al. 2012). However, available data with longer time series would be necessary to perform such an analysis in the Antisana region. These techniques could be further improved by defining climate subregions with the same climate characteristics. Unfortunately, such a subregion classification would require a longer time-period and a more homogeneous in situ station distribution that what is available now. The spatial CDF-t method could also be tested and improved in other regions of the tropical Andes with a similar spatial climate complexity but with a different temporal variability, such as regions of the Peruvian or Bolivian Andes where only one precipitation season occurs during the year. Since the CDF-t method was originally developed for correcting future predictions, this method could be adapted to correct future simulations.

28

References

Antoniadis, A., C. Helbert, C. Prieur, and L. Viry, 2012: Spatio-temporal metamodeling for West African monsoon. *Environmetrics*, **23 (1)**, 24–36, doi:10.1002/env.1134, URL https://hal.archives-ouvertes.fr/hal-00551303, special Issue: Spatio-Temporal Stochastic Modelling (METMAV).

Bai, L., S. Chunxiang, L. Li, Y. Yang, and J. Wu, 2018: Accuracy of CHIRPS satellite-rainfall products over mainland china. *Remote Sensing*, **10 (3)**, 362, doi:10.3390/rs10030362, URL https://doi.org/10.3390/rs10030362.

Basantes-Serrano, R., 2015: Evolution of glaciers in the Ecuadorian Andes since the 1950s and its contribution to the study of the climate change in the inner tropics. Theses, Université Grenoble Alpes, URL https://tel.archives-ouvertes.fr/tel-01219778.

Bendix, J., and W. Lauer, 1992: Die Niederschlagsjahreszeiten in Ecuador und ihre klimadynamische interpretation. *Erdkunde*, **46 (118-134)**.

Buytaert, W., R. Celleri, P. Willems, B. D. Bièvre, and G. Wyseure, 2006: Spatial and temporal rainfall variability in mountainous areas: A case study from the south ecuadorian andes. *Journal of Hydrology*, **329 (3-4)**, 413–421, doi:https://doi.org/10.1016/j.jhydrol.2006.02.031, URL http://www.sciencedirect.com/science/article/pii/S0022169406001144.

Buytaert, W., S. Moulds, L. Acosta, B. D. Bièvre, C. Olmos, M. Villacis, C. Tovar, and K. M. J. Verbist, 2017: Glacial melt content of water use in the tropical Andes. *Environmental Research Letters*, **12 (11)**, 114 014, URL http://stacks.iop.org/1748-9326/12/i=11/a=114014.

Cannon, A. J., 2017: Multivariate quantile mapping bias correction: an N-dimensional probability density function transform for climate model simulations of multiple variables. *Climate Dynamics*, 1–19, doi:10.1007/s00382-017-3580-6, URL http://dx.doi.org/10.1007/s00382-017-3580-6.

Chevallier, P., B. Pouyaud, W. Suarez, and T. Condom, 2011: Climate change threats to environment in the tropical Andes : glaciers and water resources. *Regional Environmental Change*, **11**, S179–S187, doi:10.1007/s10113-010-0177-6, URL http://www.documentation.ird.fr/hor/fdi:010052664.

Climate Hazard Group, 1981: CHIRPS satellite product. [Online; accessed 27-May-2017], http://chg.geog.ucsb.edu/data/chirps/.

Colette, A., R. Vautard, and M. Vrac, 2012: Regional climate downscaling with prior statistical correction of the global climate forcing. *Geophysical Research Letters*, **39 (13)**, doi:10.1029/2012GL052258, URL http://dx.doi.org/10.1029/2012GL052258, l13707.

Déqué, M., 2007: Frequency of precipitation and temperature extremes over France in an anthropogenic scenario: Model results and statistical correction according to observed values. *Global*

634   *and Planetary Change*, **57**, 16–26, doi:10.1016/j.gloplacha.2006.11.030.

635   Dudhia, J., 1989: Numerical Study of Convection observed during the Winter Monsoon

636   Experiment Using a Mesoscale Two-Dimensional Model. *Journal of the Atmospheric*

637   *Sciences*, **46 (20)**, 3077–3107, doi:10.1175/1520-0469(1989)046⟨3077:NSOCOD⟩2.0.CO;2,

638   URL https://doi.org/10.1175/1520-0469(1989)046⟨3077:NSOCOD⟩2.0.CO;2, https://doi.org/

639   10.1175/1520-0469(1989)046⟨3077:NSOCOD⟩2.0.CO;2.

640   Egger, J., and Coauthors, 2005: Diurnal Circulation of the Bolivian Altiplano. Part I: Observations.

641   *Monthly Weather Review*, **133 (4)**, 911–924, doi:10.1175/MWR2894.1, URL https://doi.org/10.

642   1175/MWR2894.1, https://doi.org/10.1175/MWR2894.1.

643   Espinoza, J. C., S. Chavez, J. Ronchail, C. Junquas, K. Takahashi, and W. Lavado, 2015: Rainfall

644   hotspots over the southern tropical Andes: Spatial distribution, rainfall intensity, and relations

645   with large-scale atmospheric circulation. *Water Resources Research*, **51 (5)**, 3459–3475, doi:

646   10.1002/2014WR016273, URL http://dx.doi.org/10.1002/2014WR016273.

647   Espinoza, J. C., J. Ronchail, J. L. Guyot, G. Cochonneau, F. Naziano, W. Lavado, and P. Vauchel,

648   2009: Spatio-temporal rainfall variability in the Amazon basin countries (Brazil, Peru, Bolivia,

649   Colombia, and Ecuador). *International Journal of Climatology*, **29 (11)**, 1574–1594.

650   Espinoza, J. C., J. Ronchail, J. L. Guyot, C. Junquas, P. Vauchel, W. Lavado, G. Drapeau, and

651   R. Pombosa, 2011: Climate variability and extreme drought in the upper Solimes River (western

652   Amazon Basin): Understanding the exceptional 2010 drought. *Geophysical Research Letters*,

653   **38 (13)**, doi:10.1029/2011GL047862, URL http://dx.doi.org/10.1029/2011GL047862, l13406.

654   Farr, T. G., and Coauthors, 2007: The Shuttle Radar Topography Mission. *Reviews of Geophysics*,

655   **45 (2)**, doi:10.1029/2005RG000183, URL http://dx.doi.org/10.1029/2005RG000183, rG2004.

Favier, V., P. Wagnon, J. P. Chazarin, L. Maisincho, and A. Coudrain, 2004: One-year measurements of surface heat budget on the ablation zone of Antizana Glacier 15, Ecuadorian Andes. *Journal of Geophysical Research*.

Forland, E., and Coauthors, 1996: Manual for operational correction of Nordic precipitation data. Rep 24/96. Oslo Norwegian Meteorological Institute.

Francou, B., M. Vuille, V. Favier, and B. Cáceres, 2004: New evidence for an ENSO impact on low latitude glaciers: Antizana 15, Andes of Ecuador. *Journal of Geophysical Research: Atmospheres*, **109 (D18)**, doi:10.1029/2003JD004484, URL https://agupubs.onlinelibrary.wiley.com/doi/abs/10.1029/2003JD004484, https://agupubs.onlinelibrary.wiley.com/doi/pdf/10.1029/2003JD004484.

Funk, C., and Coauthors, 2015: The climate hazards infrared precipitation with stations: a new environmental record for monitoring extremes. *Scientific Data 2*, **(150066)**, doi:http://doi.org/10.1038/sdata.2015.66.

Garreaud, R., 1999: Multiscale Analysis of the Summertime Precipitation over the Central Andes. *Monthly Weather Review*, **127 (5)**, 901–921, doi:10.1175/1520-0493(1999)127⟨0901:MAOTSP⟩2.0.CO;2, URL https://doi.org/10.1175/1520-0493(1999)127⟨0901:MAOTSP⟩2.0.CO;2, https://doi.org/10.1175/1520-0493(1999)127⟨0901:MAOTSP⟩2.0.CO;2.

Gräler, B., E. Pebesma, and G. Heuvelink, 2016: Spatio-Temporal Interpolation using gstat. *The R Journal*, **8**, 204–218, URL https://journal.r-project.org/archive/2016-1/na-pebesma-heuvelink.pdf.

Gräler, B., M. Rehr, L. Gerharz, and E. Pebesma, 2012: Spatio-temporal analysis and interpolation of PM10 measurements in Europe for 2009. *ETC/ACM Technical Paper*, **8**, 1–29.

Grell, G. A., and D. Dévényi, 2002: A generalized approach to parameterizing convection combining ensemble and data assimilation techniques. *Geophysical Research Letters*, **29 (14)**, 38–1–38–4, doi:10.1029/2002GL015311, URL https://agupubs. onlinelibrary.wiley.com/doi/abs/10.1029/2002GL015311, https://agupubs.onlinelibrary.wiley. com/doi/pdf/10.1029/2002GL015311.

Hall, M., and Coauthors, 2012: Los peligros volcánicos asociados con el Antisana. Corporación Editora Nacional IG-EPN IRD.

Hanchoowong, R., U. Weesakul, and S. Chumchean, 2012: Bias correction of radar rainfall estimates based on a geostatistical technique. *ScienceAsia*, **38**, 373–385.

Herold, N., A. Behrangi, and L. V. Alexander, 2017: Large uncertainties in observed daily precipitation extremes over land. *Journal of Geophysical Research: Atmospheres*, **122 (2)**, 668–681, doi:10.1002/2016JD025842, URL https://agupubs.onlinelibrary.wiley.com/doi/abs/10. 1002/2016JD025842, https://agupubs.onlinelibrary.wiley.com/doi/pdf/10.1002/2016JD025842.

Hong, S.-Y., Y. Noh, and J. Dudhia, 2006: A New Vertical Diffusion Package with an Explicit Treatment of Entrainment Processes. *Monthly Weather Review*, **134 (9)**, 2318–2341, doi:10.1175/MWR3199.1, URL https://doi.org/10.1175/MWR3199.1, https://doi.org/10.1175/ MWR3199.1.

IPCC, 2013: *Summary for Policymakers*, book section SPM, 130. Cambridge University Press, Cambridge, United Kingdom and New York, NY, USA, doi:10.1017/CBO9781107415324.004, URL www.climatechange2013.org.

Jiménez, P. A., and J. Dudhia, 2012: Improving the Representation of Resolved and Unresolved Topographic Effects on Surface Wind in the WRF Model. *Journal of Applied Meteorology and*

Climatology, **51 (2)**, 300–316, doi:10.1175/JAMC-D-11-084.1, URL https://doi.org/10.1175/JAMC-D-11-084.1, https://doi.org/10.1175/JAMC-D-11-084.1.

Junquas, C., K. Takahashi, T. Condom, J.-C. Espinoza, S. Chavez, J.-E. Sicart, and T. Lebel, 2017: Understanding the influence of orography on the precipitation diurnal cycle and the associated atmospheric processes in the central Andes. *Climate Dynamics*, doi:10.1007/s00382-017-3858-8, URL https://doi.org/10.1007/s00382-017-3858-8.

Kendall, M., 1948: *Rank correlation methods*. Griffin, London.

Kwiatkowski, D., P. Phillips, P. Schmidt, and Y. Shin, 1992: Testing the null hypothesis of stationarity against the alternative of a unit root: How sure are we that economic time series have a unit root? *Journal of Econometrics*, **54 (1-3)**, 159–178, URL https://EconPapers.repec.org/RePEc:eee:econom:v:54:y:1992:i:1-3:p:159-178.

Laraque, A., J. Ronchail, G. Cochonneau, R. Pombosa, and J. L. Guyot, 2007: Heterogeneous Distribution of Rainfall and Discharge Regimes in the Ecuadorian Amazon Basin. *Journal of Hydrometeorology*, **8 (6)**, 1364–1381, doi:10.1175/2007JHM784.1, URL https://doi.org/10.1175/2007JHM784.1, https://doi.org/10.1175/2007JHM784.1.

Lin, Y.-L., R. D. Farley, and H. D. Orville, 1983: Bulk Parameterization of the Snow Field in a Cloud Model. *Journal of Climate and Applied Meteorology*, **22 (6)**, 1065–1092, doi:10.1175/1520-0450(1983)022⟨1065:BPOTSF⟩2.0.CO;2, URL https://doi.org/10.1175/1520-0450(1983)022⟨1065:BPOTSF⟩2.0.CO;2, https://doi.org/10.1175/1520-0450(1983)022⟨1065:BPOTSF⟩2.0.CO;2.

Ly, S., C. Charles, and A. Degré, 2011: Geostatistical interpolation of daily rainfall at catchment scale: the use of several variogram models in the Ourthe and Ambleve catchments, Belgium.

Hydrology and Earth System Sciences, **15 (7)**, 2259–2274, doi:10.5194/hess-15-2259-2011, URL http://www.hydrol-earth-syst-sci.net/15/2259/2011/.

Mann, H. B., 1945: Nonparametric tests against trend. *Econometrica*, **13 (3)**, 245–259, URL http://www.jstor.org/stable/1907187.

Manz, B., S. Páez-Bimos, N. Horna, W. Buytaert, B. Ochoa-Tocachi, W. Lavado-Casimiro, and B. Willems, 2017: Comparative Ground Validation of IMERG and TMPA at Variable Spatiotemporal Scales in the Tropical Andes. *Journal of Hydrometeorology*, **18 (9)**, 2469–2489, doi:10.1175/JHM-D-16-0277.1, URL https://doi.org/10.1175/JHM-D-16-0277.1, https://doi.org/10.1175/JHM-D-16-0277.

Marrel, A., B. Iooss, F. Van Dorpe, and E. Volkova, 2008: An efficient methodology for modeling complex computer codes with Gaussian processes. *Computational Statistics & Data Analysis*, **52 (10)**, 4731–4744.

Maussion, F., D. Scherer, R. Finkelnburg, J. Richters, W. Yang, and T. Yao, 2011: WRF simulation of a precipitation event over the tibetan plateau, China an assessment using remote sensing and ground observations. *Hydrology and Earth System Sciences*, **15 (6)**, 1795–1817, doi:10.5194/hess-15-1795-2011, URL http://www.hydrol-earth-syst-sci.net/15/1795/2011/.

Michelangeli, P. A., M. Vrac, and H. Loukos, 2009: Probabilistic downscaling approaches: Application to wind cumulative distribution functions. *Geophysical Research Letters*, **36 (11)**, doi:10.1029/2009GL038401.

Mlawer, E., S. Taubman, P. Brown, M. Iacono, and S. Clough, 1997: Radiative transfer for inhomogeneous atmospheres: RRTM, a validated correlated-k model for the longwave. *Journal of Geophysical Research: Atmospheres*, **102**, 16, doi:10.1029/97JD00237.

Mourre, L., T. Condom, C. Junquas, T. Lebel, J. E. Sicart, R. Figueroa, and A. Cochachin, 2016: Spatio-temporal assessment of WRF, TRMM and in situ precipitation data in a tropical mountain environment (Cordillera Blanca, Peru). *Hydrology and Earth System Sciences*, **20 (1)**, 125–141, doi:10.5194/hess-20-125-2016, URL http://www.hydrol-earth-syst-sci.net/20/125/2016/.

Moya-Álvarez, A. S., D. Martínez-Castro, J. L. Flores, and Y. Silva, 2018: Sensitivity Study on the Influence of Parameterization Schemes in WRF_ ARW Model on Short- and Medium Range Precipitation Forecasts in the Central Andes of Peru. *Advances in Meteorology*, **2018**, doi:https://doi.org/10.1155/2018/1381092.

Müller, M. F., and S. E. Thompson, 2013: Bias adjustment of satellite rainfall data through stochastic modeling: Methods development and application to Nepal. *Advances in Water Resources*, **60**, 121–134.

Niu, G.-Y., and Coauthors, 2011: The community Noah land surface model with multiparameterization options (Noah-MP): 1. Model description and evaluation with local-scale measurements. *Journal of Geophysical Research: Atmospheres*, **116 (D12)**, n/a–n/a, doi:10.1029/2010JD015139, URL http://dx.doi.org/10.1029/2010JD015139, d12109.

Oakley, J., and A. O'Hagan, 2002: Bayesian inference for the uncertainty distribution of computer model outputs. *Biometrika*, **89 (4)**, 769–784, doi:10.1093/biomet/89.4.769, URL +http://dx.doi.org/10.1093/biomet/89.4.769, /oup/backfile/content_public/journal/biomet/89/4/10.1093/biomet/89.4.769/2/890769.pdf.

Ochoa, A., L. Campozano, E. Sánchez, R. Gualán, and E. Samaniego, 2016: Evaluation of downscaled estimates of monthly temperature and precipitation for a Southern Ecuador case study. *International Journal of Climatology*, **36**, 1244–1255, doi:10.5194/hess-18-3179-2014.

Ochoa, A., L. Pineda, P. Crespo, and P. Willems, 2014: Evaluation of TRMM 3B42 precipitation estimates and WRF retrospective precipitation simulation over the Pacific-Andean region of Ecuador and Peru. *Hydrol. Earth Syst. Sci.*, **18**, 3179–3193, doi:10.5194/hess-18-3179-2014.

Ouzeau, G., J.-M. Soubeyroux, M. Schneider, R. Vautard, and S. Planton, 2016: Heat waves analysis over France in present and future climate: Application of a new method on the EURO-CORDEX ensemble. *Climate Services*, **4**, 1 – 12, doi:https://doi.org/10.1016/j.cliser.2016.09.002, URL http://www.sciencedirect.com/science/article/pii/S2405880716300309.

Paccini, L., J. C. Espinoza, J. Ronchail, and H. Segura, 2018: Intraseasonal rainfall variability in the Amazon basin related to largescale circulation patterns: a focus on western AmazonAndes transition region. *International Journal of Climatology*, **38 (5)**, 2386–2399, doi:10.1002/joc.5341, URL https://rmets.onlinelibrary.wiley.com/doi/abs/10.1002/joc.5341, https://rmets.onlinelibrary.wiley.com/doi/pdf/10.1002/joc.5341.

Paciorek, C. J., and M. J. Schervish, 2006: Spatial modelling using a new class of nonstationary covariance functions. *Environmetrics*, **17 (5)**, 483–506, doi:10.1002/env.785, URL http://dx.doi.org/10.1002/env.785.

Paredes-Trejo, F. J., H. Barbosa, and T. Lakshmi Kumar, 2017: Validating CHIRPS-based satellite precipitation estimates in Northeast Brazil. *Journal of Arid Environments*, **139**, 26 – 40, doi:https://doi.org/10.1016/j.jaridenv.2016.12.009, URL http://www.sciencedirect.com/science/article/pii/S014019631630235X.

Paulson, C. A., 1970: The Mathematical Representation of Wind Speed and Temperature Profiles in the Unstable Atmospheric Surface Layer. *Journal of Applied Meteorology*, **9 (6)**, 857–861, doi:10.1175/1520-0450(1970)009⟨0857:TMROWS⟩2.0.CO;2,

URL https://doi.org/10.1175/1520-0450(1970)009⟨0857:TMROWS⟩2.0.CO;2, https://doi.org/ 10.1175/1520-0450(1970)009⟨0857:TMROWS⟩2.0.CO;2.

Pebesma, E. J., 2004: Multivariable geostatistics in S: the gstat package. *Computers and Geosciences*, **30**, 683–691.

Piani, C., G. Weedon, M. Best, S. Gomes, P. Viterbo, S. Hagemann, and J. Haerter, 2010: Statistical bias correction of global simulated daily precipitation and temperature for the application of hydrological models. *Journal of Hydrology*, **395 (3)**, 199 – 215, doi:https:// doi.org/10.1016/j.jhydrol.2010.10.024, URL http://www.sciencedirect.com/science/article/pii/ S0022169410006475.

Pouget, J.-C., D. Proano, A. Vera, M. Villacis, T. Condom, M. Escobar, P. Le Goulven, and R. Calvez, 2017: Modélisation glacio-hydrologique et gestion des ressources en eau dans les Andes équatoriennes : l'exemple de Quito. *Hydrological Sciences Journal = Journal des Sciences Hydrologiques*, **62**, 431–446, doi:10.1080/02626667.2015.1131988, URL http: //www.documentation.ird.fr/hor/fdi:010069651.

R Core Team, 2015: *R: A Language and Environment for Statistical Computing*. Vienna, Austria, R Foundation for Statistical Computing, URL https://www.R-project.org.

Rabatel, A., and Coauthors, 2013: Current state of glaciers in the tropical andes: a multi-century perspective on glacier evolution and climate change. *The Cryosphere*, **7 (1)**, 81–102, doi:10. 5194/tc-7-81-2013, URL https://www.the-cryosphere.net/7/81/2013/.

Rasmussen, C. E., and C. K. I. Williams, 2005: *Gaussian Processes for Machine Learning (Adaptive Computation and Machine Learning)*. The MIT Press.

Rollenbeck, R., and J. Bendix, 2011: Rainfall distribution in the Andes of southern Ecuador derived from blending weather radar data and meteorological field observations. **99**, 277–289.

Rossel, F., P. Le Goulven, and E. Cadier, 1999: Repartition spatiale de linfluence de lENSO sur les precipitations annuelles en equateur. *Revue des Sciences de l'Eau*, **(12)**, 183–200.

Sicart, J., R. Hock, P. Ribstein, M. Litt, and E. Ramirez, 2011: Analysis of seasonal variations in mass balance and meltwater discharge of the Tropical Zongo Glacier by application of a distributed energy balance model. *J. Geophys. Res.*, **116**, doi:10.1029/2010JD015105.

Skamarock, W. C., and Coauthors, 2008: A description of the Advanced Research WRF Version 3. Tech. rep., National Center for Atmospheric Research, 1–113 pp.

Vera, C., and Coauthors, 2006: Toward a Unified View of the American Monsoon Systems. *Journal of Climate*, **19 (20)**, 4977–5000, doi:10.1175/JCLI3896.1, URL https://doi.org/10.1175/JCLI3896.1, https://doi.org/10.1175/JCLI3896.1.

Vicente-Serrano, S. M., and Coauthors, 2017: The complex influence of enso on droughts in ecuador. *Climate Dynamics*, **48 (1)**, 405–427, doi:10.1007/s00382-016-3082-y, URL https://doi.org/10.1007/s00382-016-3082-y.

Vrac, M., 2015: *Statistical downscaling through CDF-transform*. URL https://cran.r-project.org/web/packages/CDFt/index.html, r package version 1.0.1.

Vrac, M., P. Drobinski, A. Merlo, M. Herrmann, C. Lavaysse, L. Li, and S. Somot, 2012: Dynamical and statistical downscaling of the French Mediterranean climate: uncertainty assessment. *Natural Hazards and Earth System Sciences*, **12 (9)**, 2769–2784, doi:10.5194/nhess-12-2769-2012, URL http://www.nat-hazards-earth-syst-sci.net/12/2769/2012/.

Vrac, M., and P. Friederichs, 2015: Multivariate-Intervariable, Spatial, and Temporal-Bias Correction. *Journal of Climate*, **28 (1)**, 218–237, doi:10.1175/JCLI-D-14-00059.1.

Vrac, M., T. Noel, and R. Vautard, 2016: Bias correction of precipitation through Singularity Stochastic Removal: Because occurrences matter. *Journal of Geophysical Research: Atmospheres*.

Vrac, M., and P. Vaittinada, 2017: Influence of Bias Correcting Predictors on Statistical Downscaling Models. *Journal of Applied Meteorology and Climatology*, **56 (1)**, 5–26, doi:10.1175/JAMC-D-16-0079.1, URL http://dx.doi.org/10.1175/JAMC-D-16-0079.1, http://dx.doi.org/10.1175/JAMC-D-16-0079.1.

Vuille, M., R. S. Bradley, and F. Keimig, 2000: Climate Variability in the Andes of Ecuador and Its Relation to Tropical Pacific and Atlantic Sea Surface Temperature Anomalies. *Journal of Climate*, **13 (14)**, 2520–2535, doi:10.1175/1520-0442(2000)013⟨2520:CVITAO⟩2.0.CO;2, URL https://doi.org/10.1175/1520-0442(2000)013⟨2520:CVITAO⟩2.0.CO;2, https://doi.org/10.1175/1520-0442(2000)013⟨2520:CVITAO⟩2.0.CO;2.

Wagnon, P., M. Lafaysse, Y. Lejeune, L. Maisincho, M. Rojas, and J. P. Chazarin, 2009: Understanding and modeling the physical processes that govern the melting of snow cover in a tropical mountain environment in Ecuador. *Journal of Geophysical Research: Atmospheres*, **114 (D19)**, doi:10.1029/2009JD012292, URL https://agupubs.onlinelibrary.wiley.com/doi/abs/10.1029/2009JD012292, https://agupubs.onlinelibrary.wiley.com/doi/pdf/10.1029/2009JD012292.

Yang, Z.-L., and Coauthors, 2011: The community noah land surface model with multiparameterization options (noah-mp): 2. evaluation over global river basins. *Journal of Geophysical Research: Atmospheres*, **116 (D12)**, n/a–n/a, doi:10.1029/2010JD015140, URL http://dx.doi.org/10.1029/2010JD015140, d12110.

Zambrano-Bigiarini, M., A. Nauditt, C. Birkel, K. Verbist, and L. Ribbe, 2017: Temporal and spatial evaluation of satellite-based rainfall estimates across the complex topographical and climatic gradients of Chile. *Hydrology and Earth System Sciences*, **21 (2)**, 1295–1320, doi: 10.5194/hess-21-1295-2017, URL https://www.hydrol-earth-syst-sci.net/21/1295/2017/.

LIST OF TABLES

TABLE 1. Description of meteorological in situ stations. Total precipitation during the 2014-2015 period at each meteorological station and total precipitation in [mm] simulated by WRF at 1 km resolution. Note that for station 12 and 18, we indicate the associated grid-point model used for the bias correction computations.

Number	Elev. [m]	Lon.	Lat.	P. Obs. [mm]	P. WRF [mm]
The Pacific coast					
2	1985	-78.78	-0.21	8656	1568
22	1110	-78.90	-0.21	8954	6892
23	2028	-78.82	-0.25	6132	2140
The Andes					
1	2843	-78.53	-0.39	2447	1475
3	3447	-78.54	-0.20	2510	2478
4	2530	-78.30	-0.10	769	659
5	3317	-78.17	-0.06	835	972
6	2625	-78.42	-0.10	831	932
7	2576	-78.32	-0.16	1221	562
8	3021	-78.42	-0.43	2403	1992
9	3276	-78.63	-0.28	2886	1082
10	3498	-78.52	-0.16	2602	2368
11	2880	-78.51	0.00	995	623
12*	2949	-78.14	0.00	1763	1835
13	2930	-78.89	-0.70	1694	2105
14	3705	-78.43	-0.56	2695	753
15	3157	-78.63	-0.72	1506	757
16	3035	-78.66	-0.83	962	839
17	4009	-78.70	-0.68	1203	1229
18*	2828	-78.23	0.00	1080	1327
20	2487	-78.43	-0.18	1699	948
21	3218	-78.54	-0.09	1824	695
24	3528	-78.66	-0.62	1989	690
26	4812	-78.15	-0.47	2255	2062
The Amazon					
19	2390	-77.93	-0.67	8276	2297
25	1700	-77.82	-0.39	6261	1186

TABLE 2. Cross-validation leave-one-out results of annual precipitation for the four Gaussian Process models over the WRF bias proposed with four diferent drifts The criteria are calculated for the 2014 and 2015 periods, separately.

|	2014				2015			
	Bias	RMSE	Correlation	Q_2	Bias	RMSE	Correlation	Q_2
WRF	1.77	2.89	0.59		2.19	3.67	0.65	
GP+longitude+latitude+alt.	1.71	2.31	0.71	0.44	1.56	2.14	0.80	0.65
GP+longitude+latitude	**1.48**	**2.14**	**0.76**	**0.56**	**1.31**	**2.08**	**0.84**	0.71
GP+longitude	1.50	**2.14**	**0.76**	0.49	1.32	2.11	**0.84**	0.64
GP+elevation	1.68	2.30	0.72	**0.56**	1.72	2.29	0.78	0.70

LIST OF FIGURES

FIG. 1. Map of the region under study and INAMHI stations. The stations of each region (Pacific coast, Andes and Amazon) are marked with three geometric figures: rectangles for the Pacific coast, circles for the Andes and triangles for the Amazon. The color figures indicate the mean daily precipitation [mm day^{-1}] during the 2014-2015 period. The contour interval is 1000 m. Note that for station 12 and 18, we indicate the associated grid-point model used for the bias correction computations.
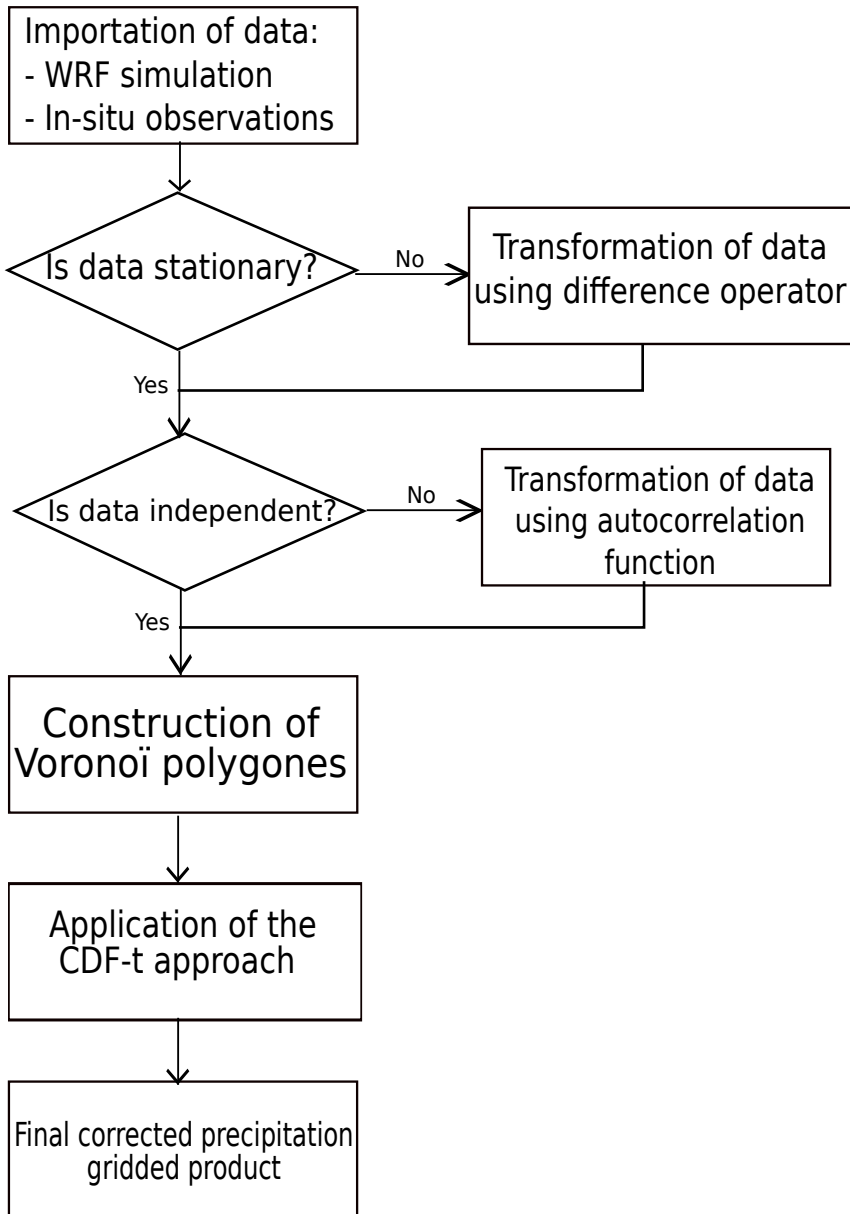
46
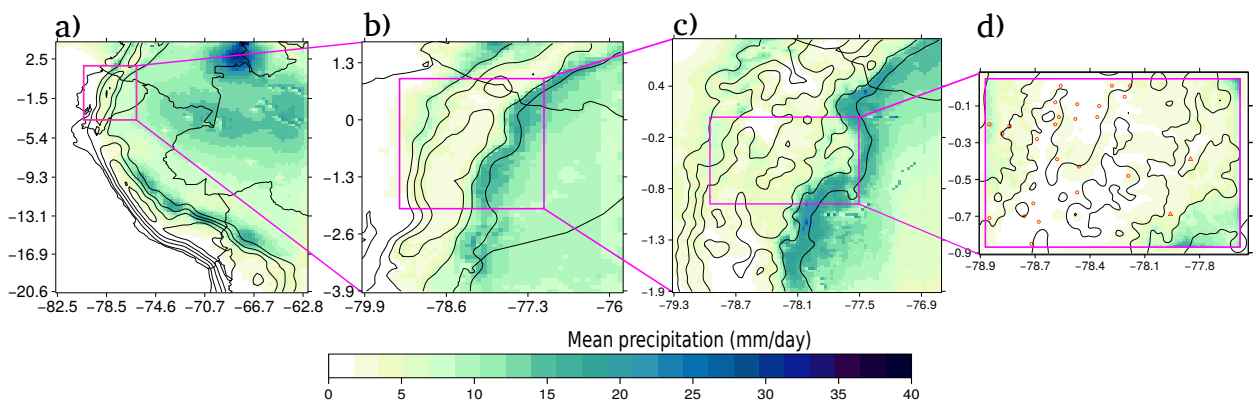
FIG. 2. Mean daily precipitation [mm day^{-1}] during the 2014-2015 period of the four nested domains of the WRF simulation a) WRF 27 km, b) WRF 9 km, c) WRF 3 km and d) WRF 1 km. Figure d) shows the exact WRF domain, the WRF domain without the lateral boundary zone (purple box) and the stations (red dots). Note that for station 12 and 18, we indicate the associated grid-point model used for the bias correction computations.
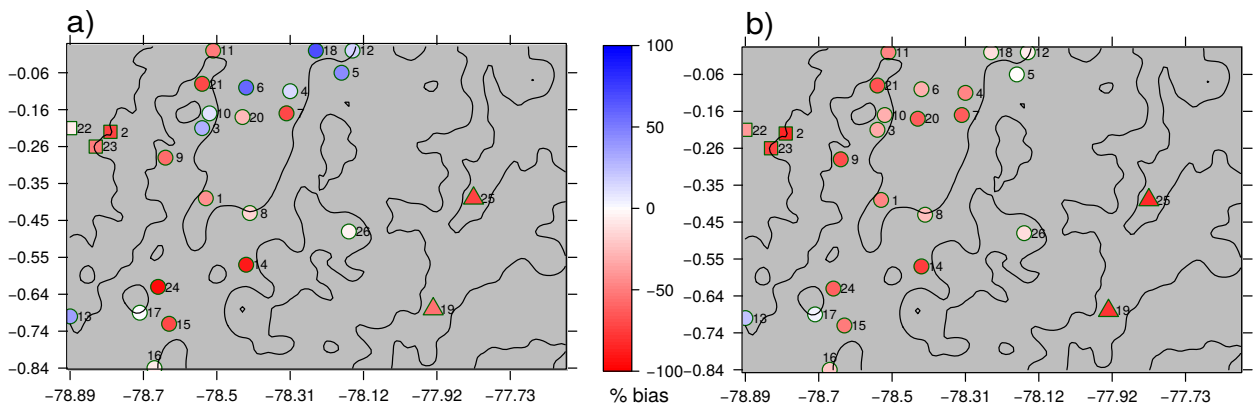
FIG. 3. WRF precipitation relative biases for the **a)** 2014 and **b)** 2015 (% of relative error). Note that for station 12 and 18, we indicate the associated grid-point model used for the bias correction computations.
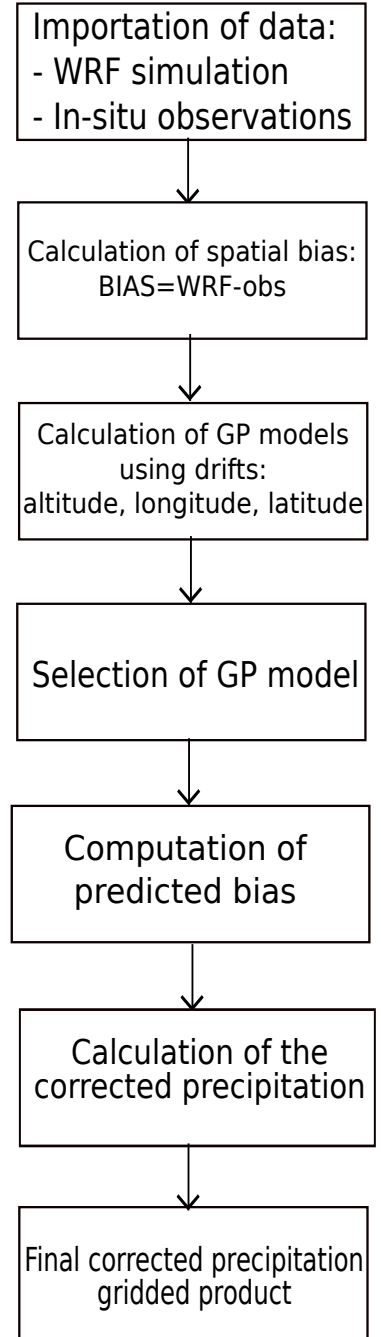
a)

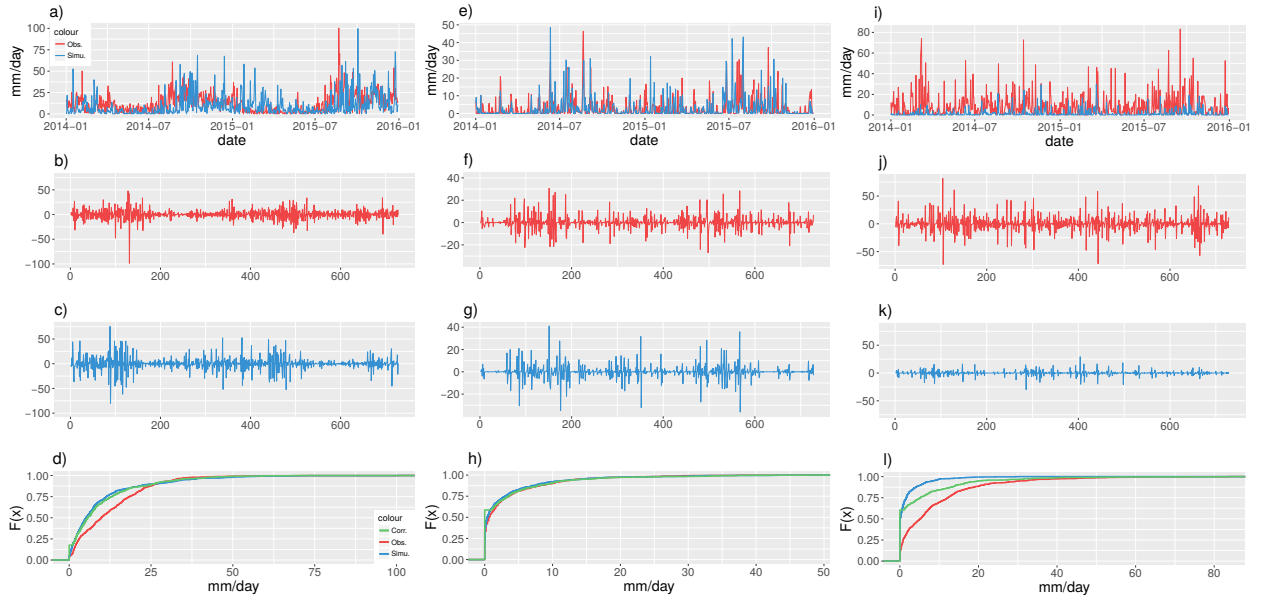Importation of data:
- WRF simulation
- In-situ observations

Is data stationary? → No → Transformation of data using difference operator

Yes

Is data independent? → No → Transformation of data using autocorrelation function

Yes

Construction of Voronoï polygones

Application of the CDF-t approach

Final corrected precipitation gridded product

b)

Importation of data:
- WRF simulation
- In-situ observations

Calculation of spatial bias: BIAS=WRF-obs

Calculation of GP models using drifts: altitude, longitude, latitude

Selection of GP model

Computation of predicted bias

Calculation of the corrected precipitation

Final corrected precipitation gridded product

FIG. 4. Flowchart for the two approaches **a)** Spatial CDF-t and **b)** Gaussian process model.

FIG. 5. Time series treatment for a Pacific coast station (station 22), an Andes station (Antisana station 26), and Amazon station (station 25). **a)** Original time series (X_t in red and Y_t in blue) for the Pacific coast station (*resp.*, **e** and **i**, for the Andes station and the Amazon station), **b)** differentiated observed time series ΔY_t (*resp.*, **f** and **j**, for the Andes station and the Amazon station), **c)** differentiated simulated time series ΔX_t (*resp.*, **g** and **k**, for the Andes station and the Amazon station) and **d)** CDFs of observation (obs.), simulation (Simu.) and CDF-t correction (Corr.) (*resp.*, **h** and **l**, for the Andes station and the Amazon station).
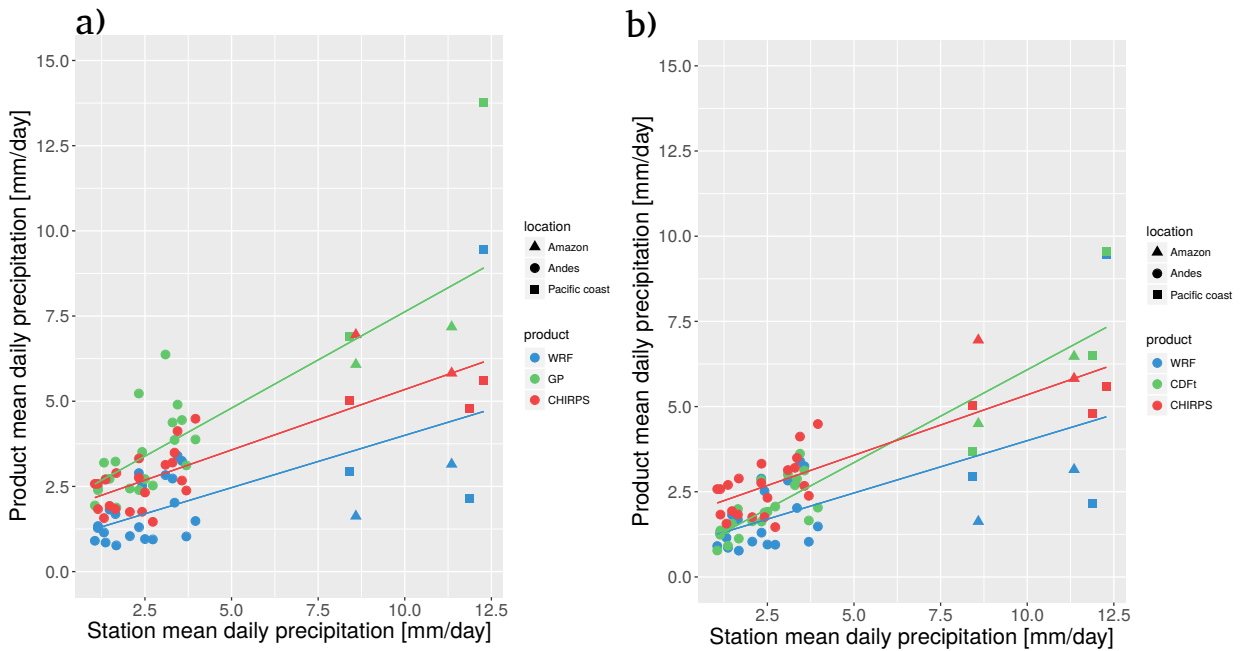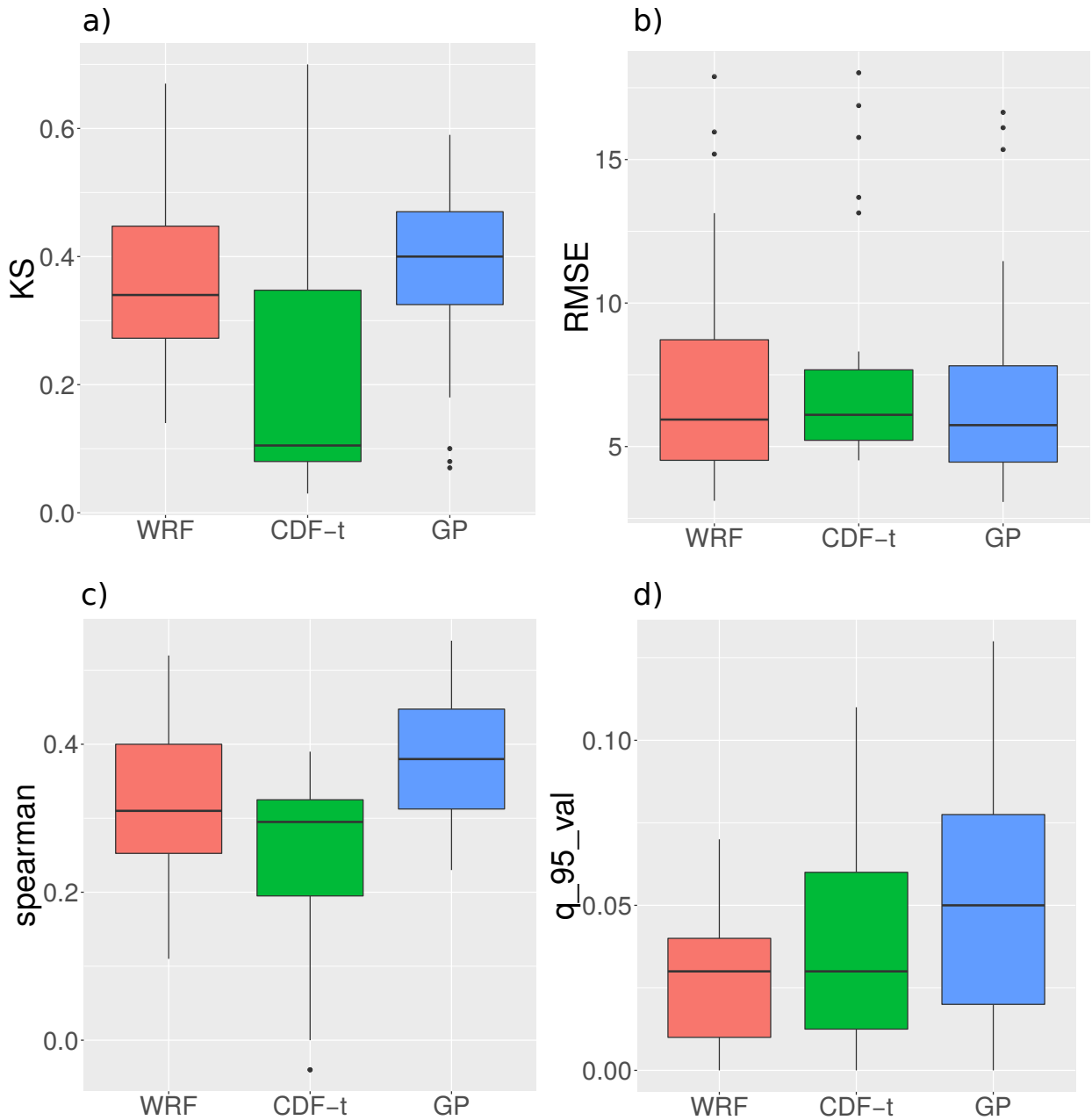
FIG. 6. Scatter plots of gridded product mean daily precipitation (CHIRPS, WRF) and a) CDF-t and b) GP

results using cross-validation versus the stations mean daily precipitation [mm day^{-1}].
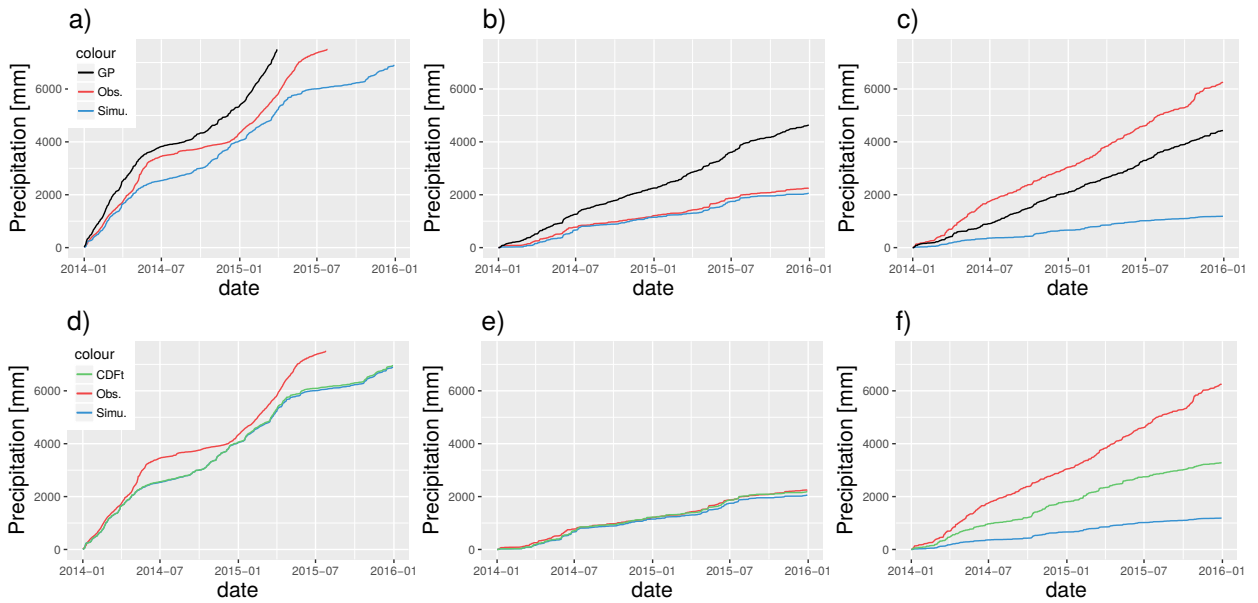
₉₃₃   FIG. 7. The accumulated precipitation [mm] of the WRF, GP (*resp.*,CDF-t) and the in situ stations of three

₉₃₄   regions. GP is evaluated in cross-validation leave-one-out. **a)** Pacific coast (station 22) for GP (*resp.*, **d** for

₉₃₅   CDF-t)**b)** Andes (station 26) for GP (*resp.*, **d** for CDF-t) **c)** Amazon (station 25) for GP (*resp.*, **d** for CDF-t).
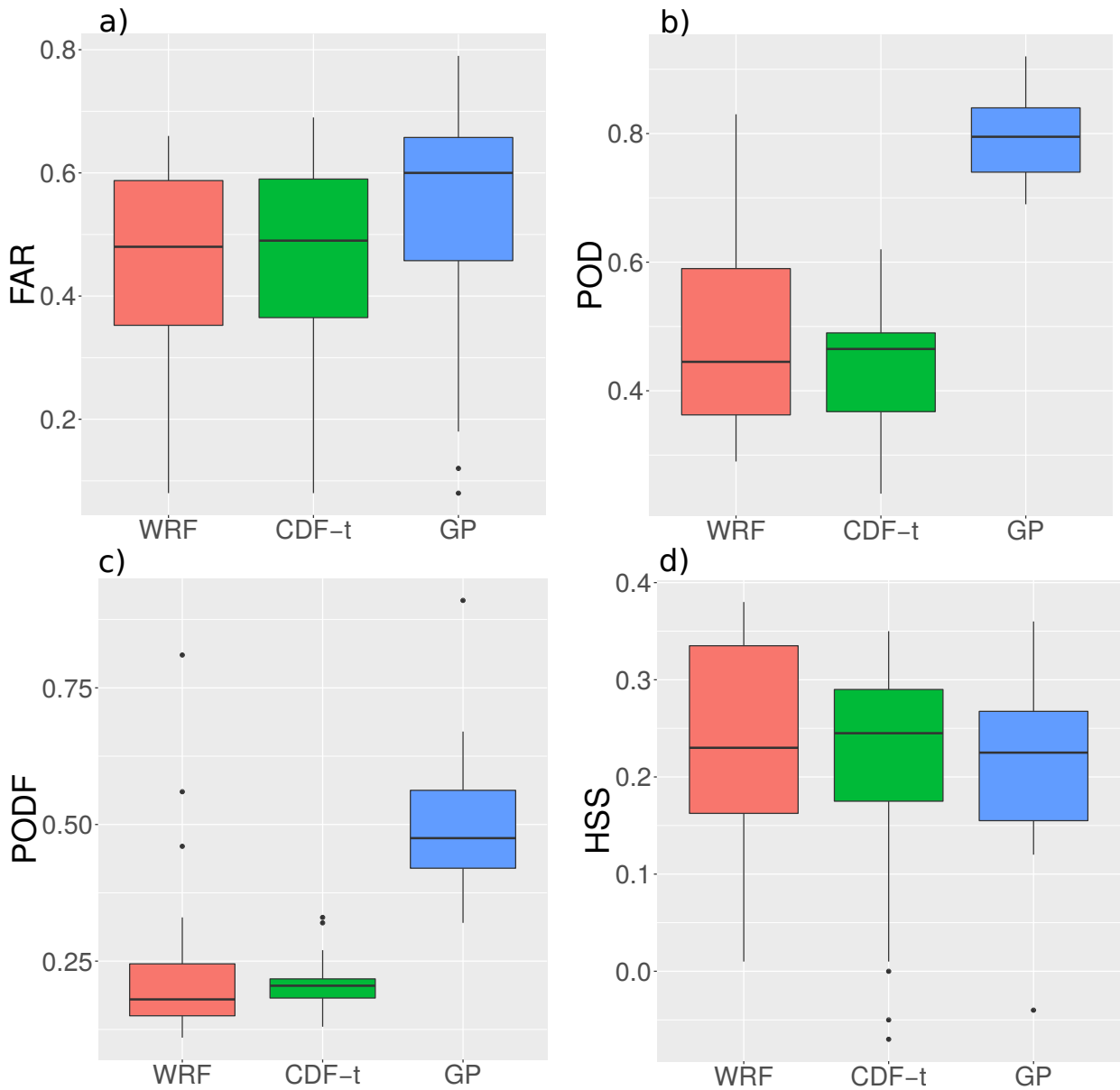
FIG. 8. Boxplots of criteria related to precipitation occurrence (rainy/non-rainy events) for three gridded products: WRF, Spatial CDF-t and GP (Gaussian Process model with drift longitude and latitude), using a cross-validation leave-one- out framework. **a)** FAR criterion (ideal value 0), **b)** POD criterion (1), **c)** PODF criterion (0) and **d)** HSS criterion (1).
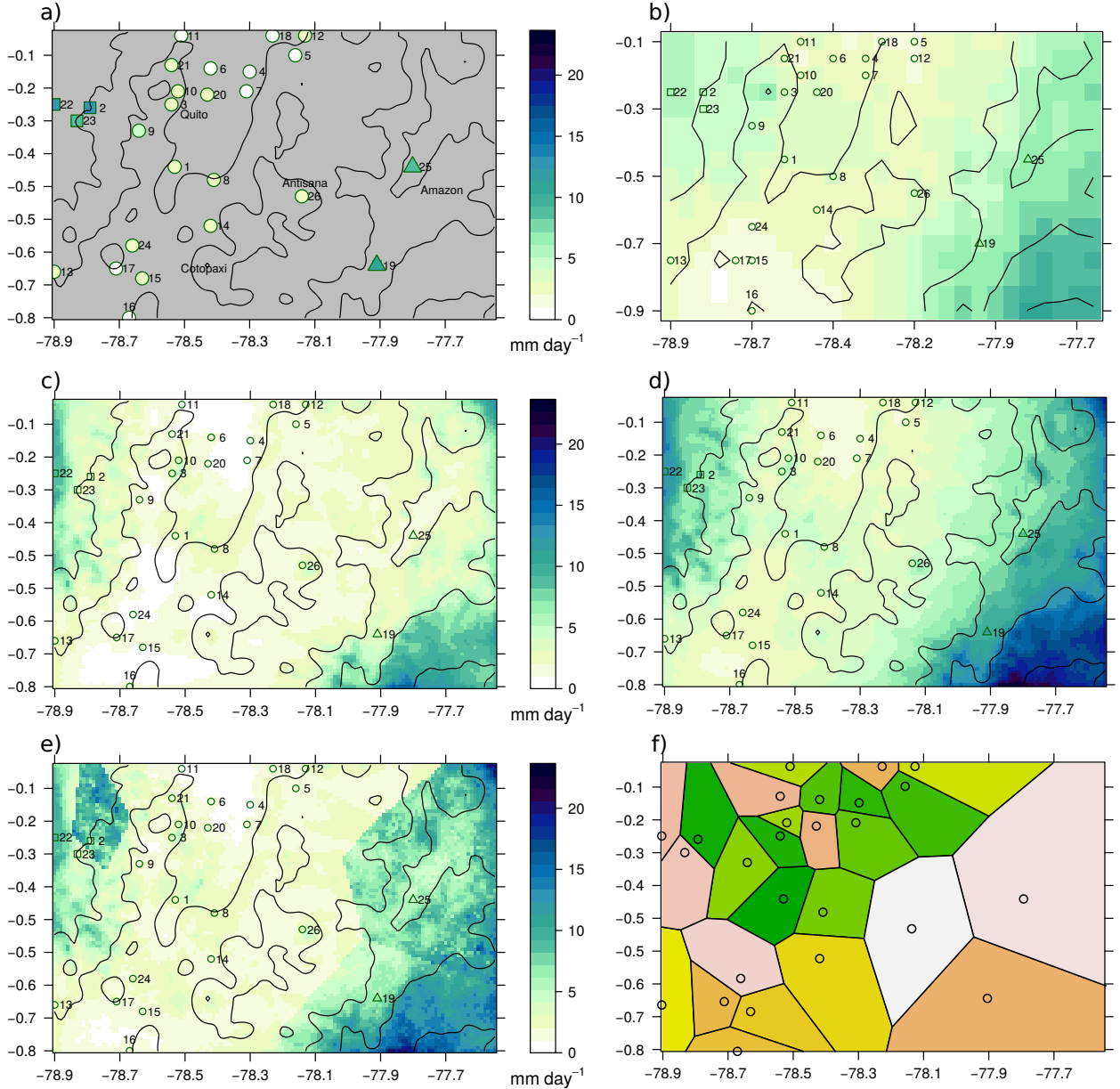
FIG. 10. Mean of daily precipitation maps [mm day^{-1}] during 2014-2015 and Voronoï diagram. **a)** Observations in situ, **b)** CHIRPS, **c)** WRF simulation, **d)** GP model, **e)** Spatial CDF-t and **f)** Voronoï diagram. The stations are represented by green circles. Note that for station 12 and 18, we indicate the associated grid-point model used for the bias correction computations.